

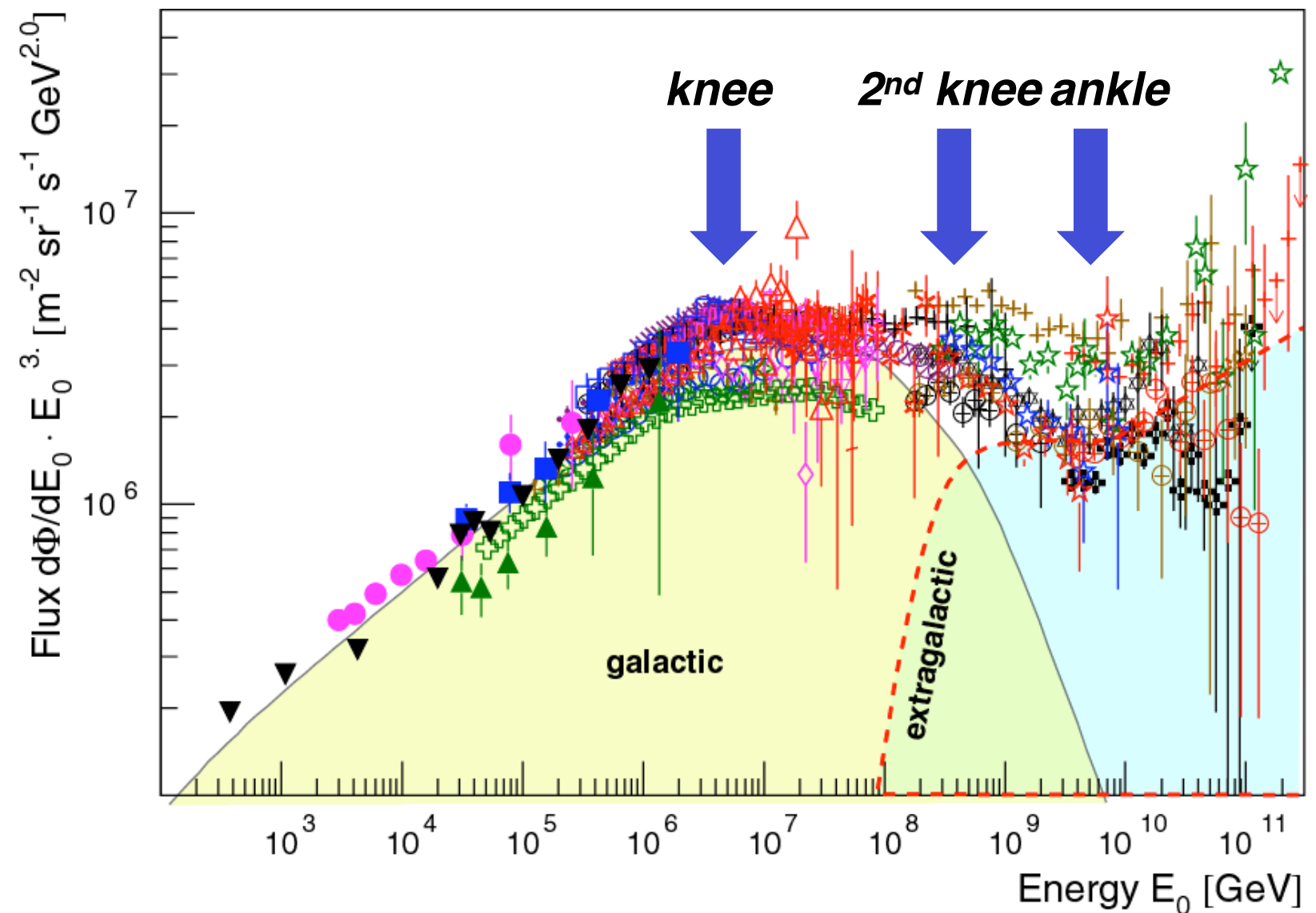
Paris
7-11 December 2020



Nikhef



Models for the knee in the energy spectrum of cosmic rays



A Matthews Heitler Model – mass resolution in EAS measurements

depth of shower maximum

$$X_{\max}^A = X_{\max}^p - X_0 \ln A$$

radiation length $X_0=36.7 \text{ g/cm}^2$

typical uncertainty

$$\Delta X_{\max} \approx 20 \text{ g/cm}^2$$

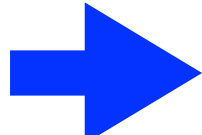
expected mass resolution


$$\Delta \ln A \approx 0.8 - 1$$

electron-muon ratio

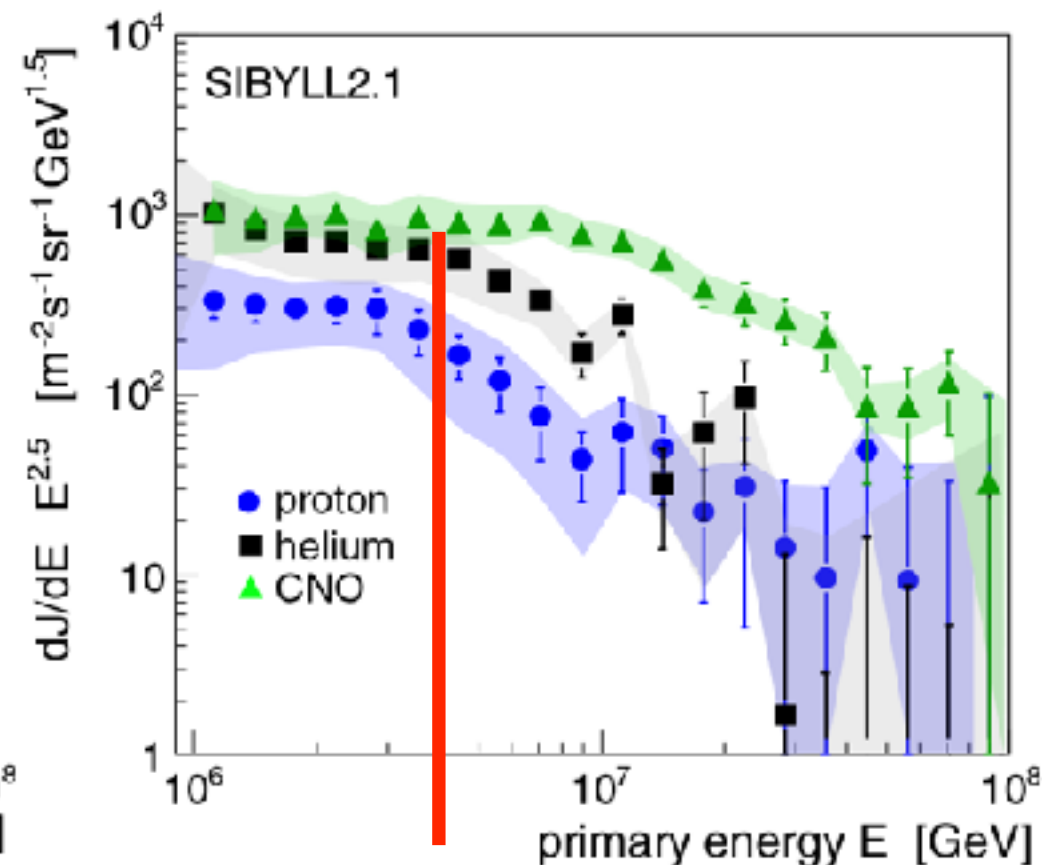
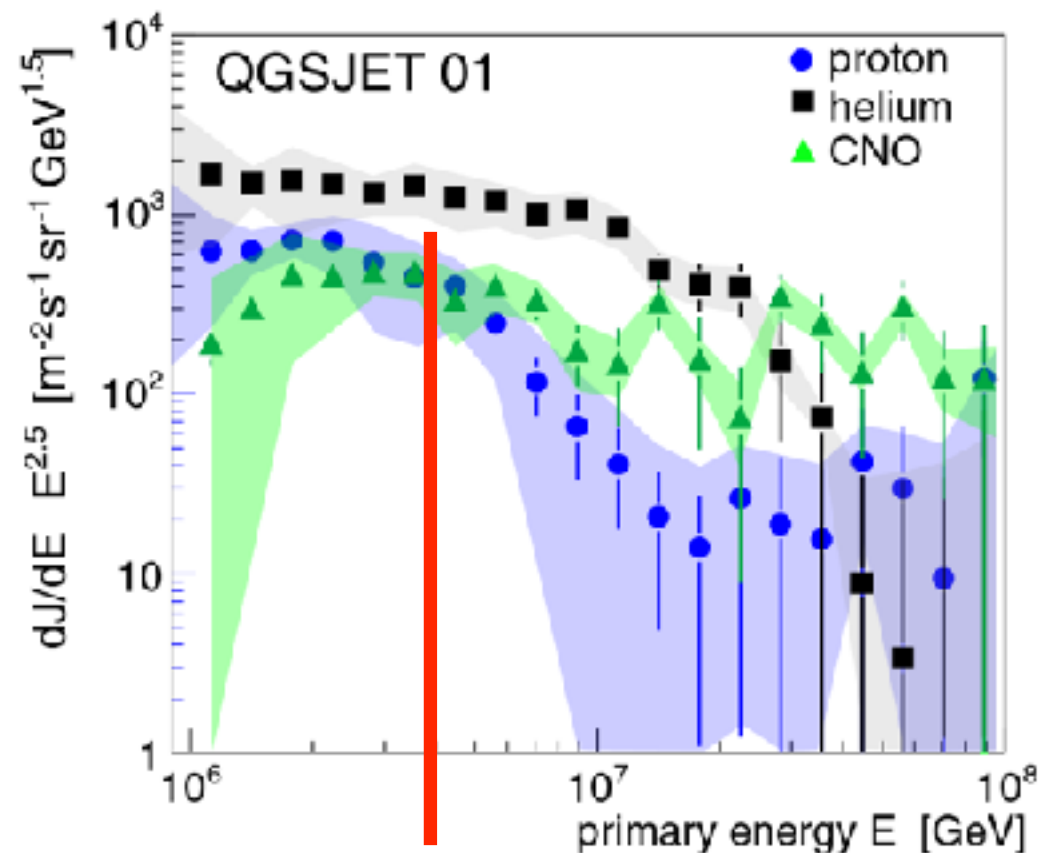
$$\lg(N_e/N_\mu) = C - 0.065 \ln A.$$

$$\Delta \frac{N_e}{N_\mu} \approx 16\% - 20\%$$



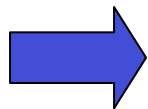
4 to 5 mass groups
p, He, CNO, (Si), Fe

KASCADE: Energy spectra for elemental groups



4 PeV

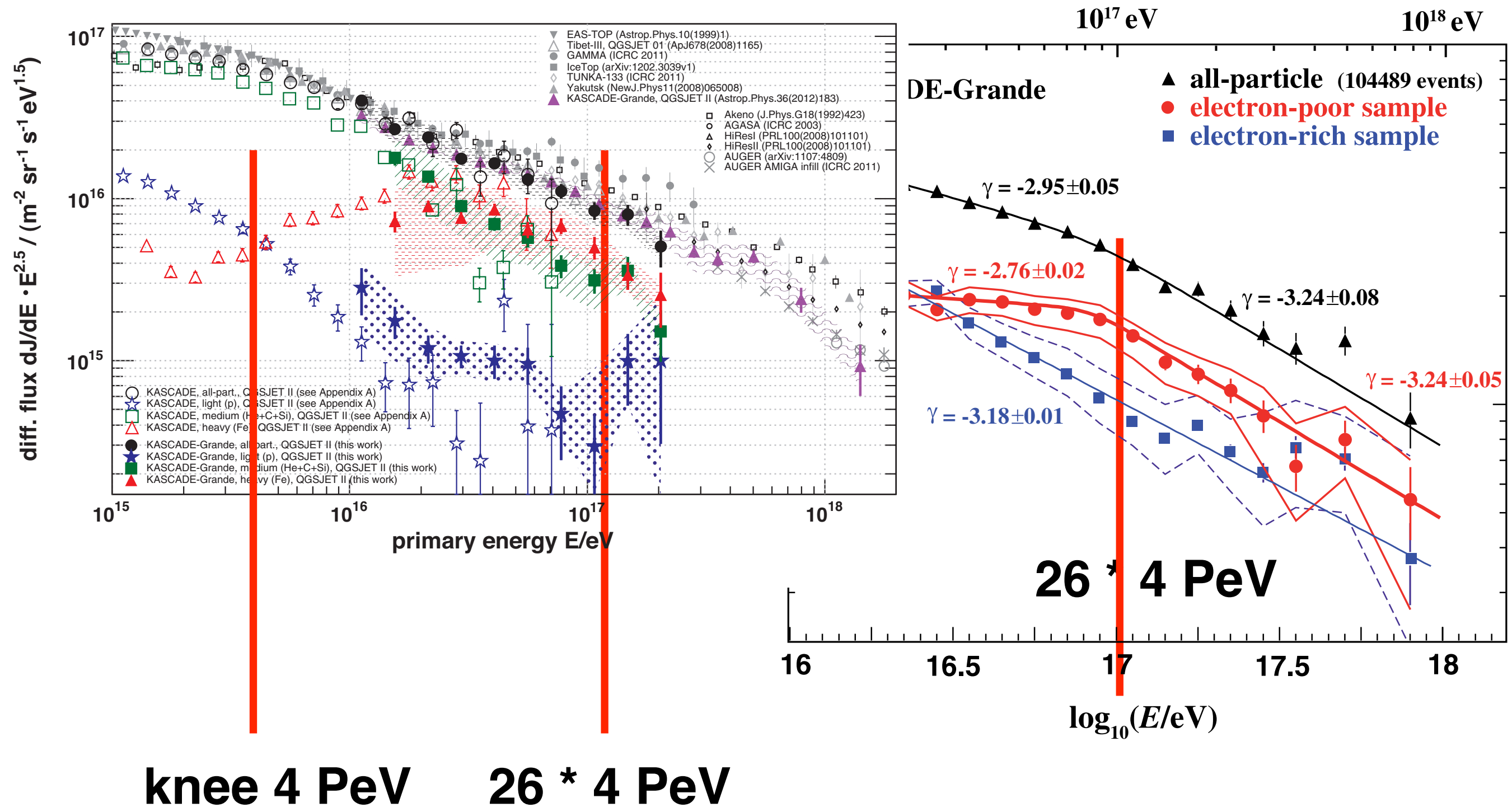
4 PeV



Knee caused by cut-off for light elements

**Astrophysical interpretation
limited by description of
interactions in the atmosphere**

KASCADE-Grande



W.D. Apel et al., PRL 107 (2011) 171104

W.D. Apel et al., Astropart. Phys 47 (2013) 54

Ice Cube - Ice Top

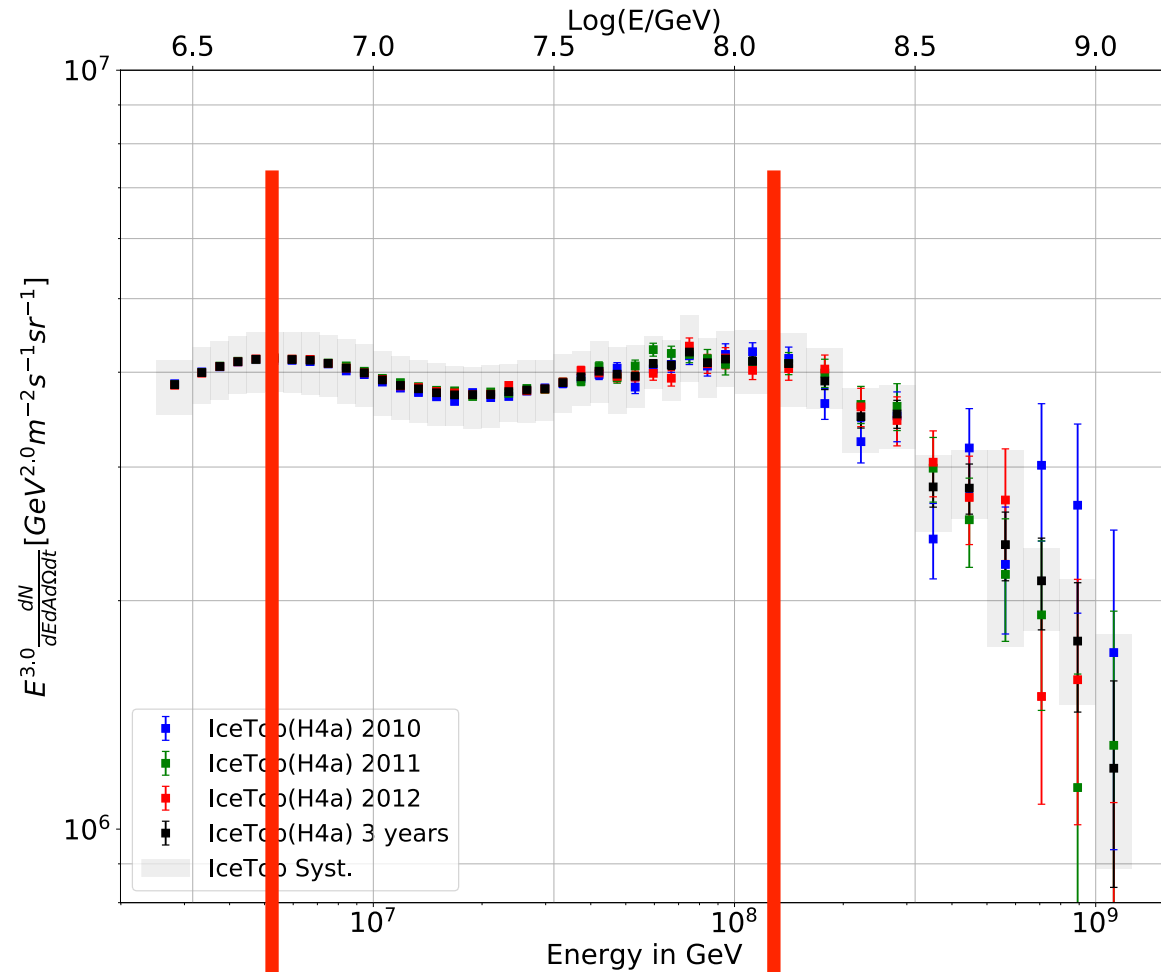


FIG. 9. All-particle energy spectrum from the IceTop-alone analysis from each of the three years, and the three years together.

~5 PeV ~26*5 PeV
Ice Top only

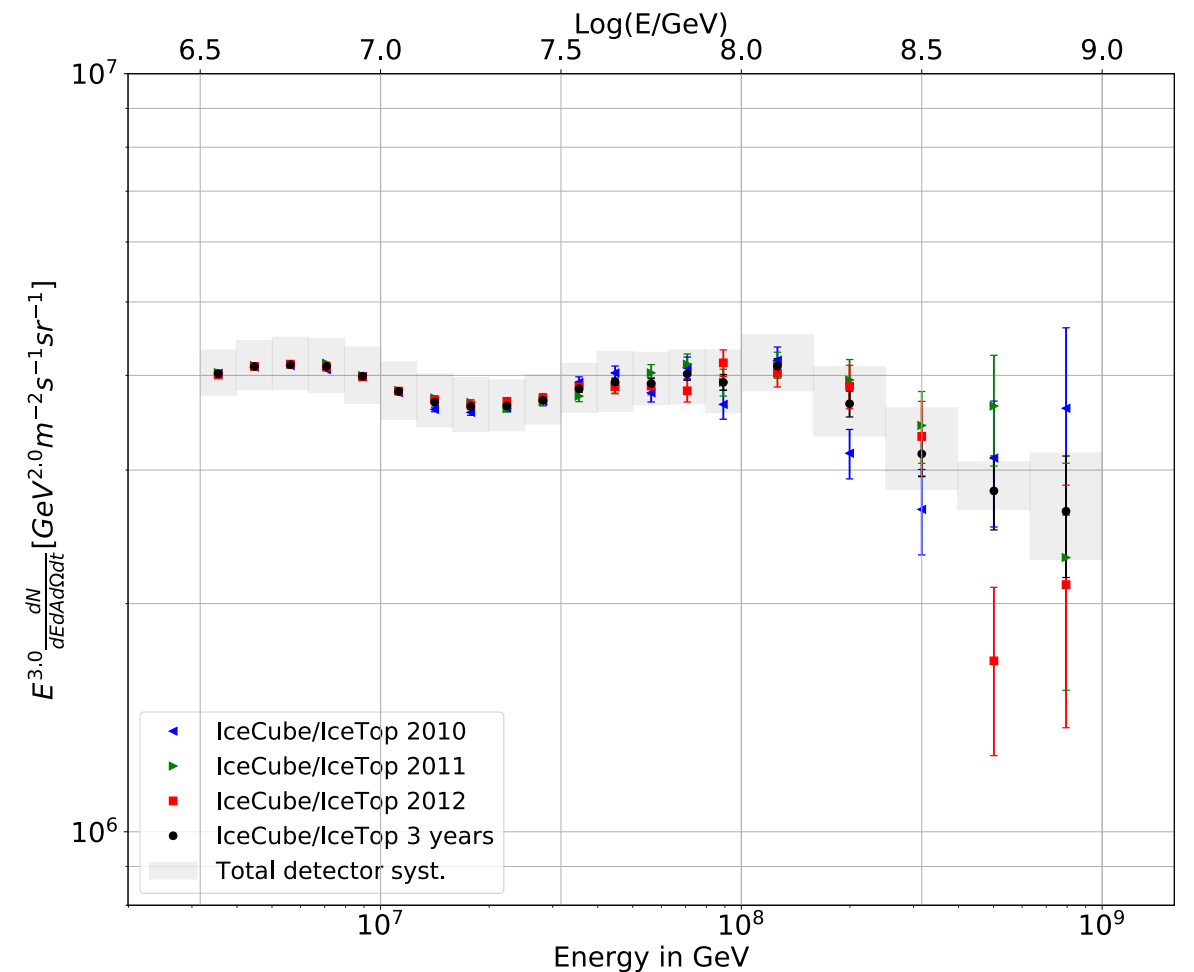


FIG. 12. All-particle energy spectrum from the coincident analysis from each of the three years analyzed individually compared to the combined result. The gray band represents the total detector uncertainty from both the IceTop and InIce arrays, as discussed in Section IV B.

combined

Ice Cube - Ice Top

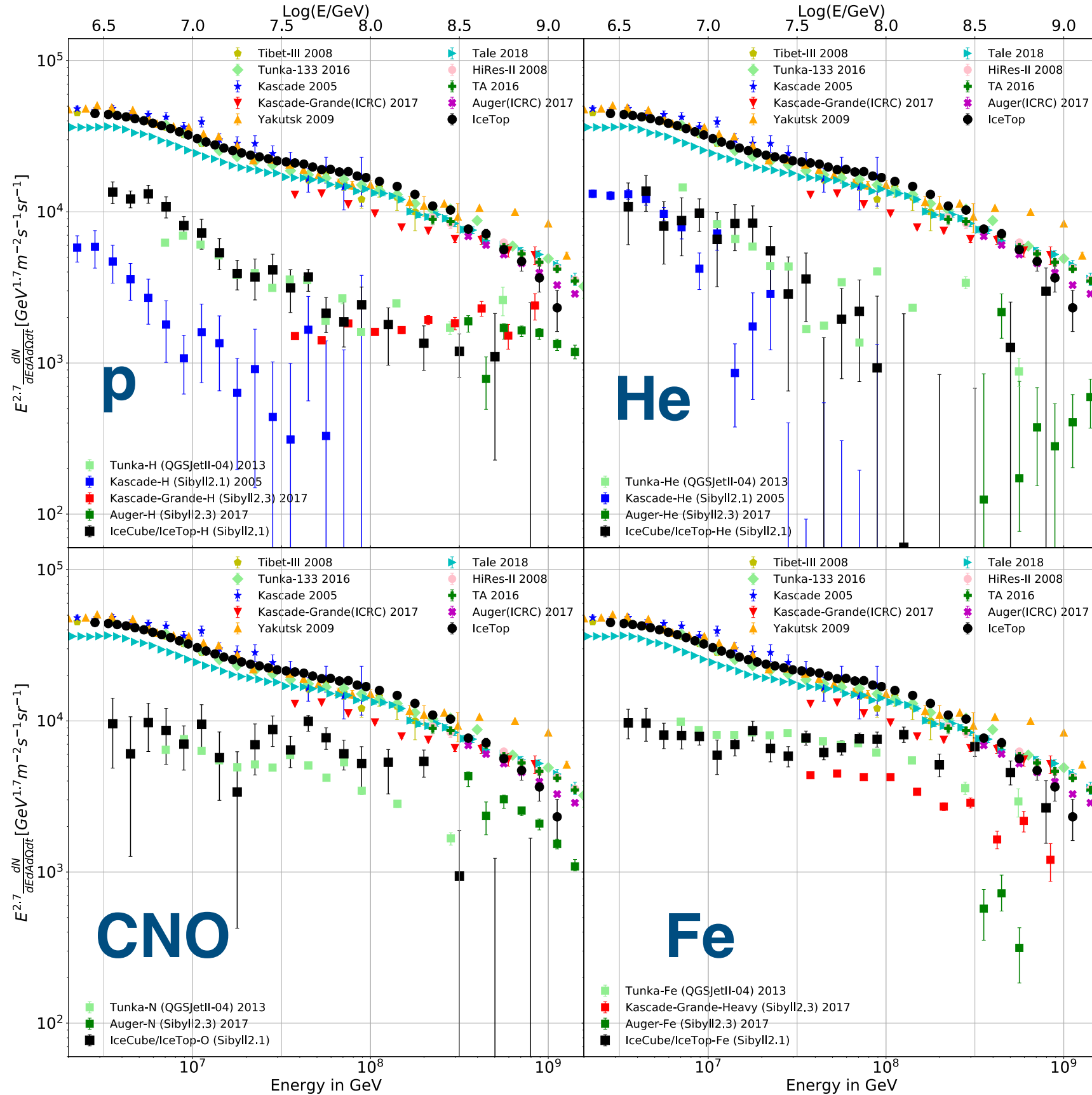


FIG. 25. Comparison of the all-particle and composition spectra of H, He, O and Fe from this analysis using Sibyll 2.1 (black) with other experiments. The data set for the all-particle spectra are taken from Tibet [42], Tunka [43], Yakutsk [44], Tale [45], Hires [46] and Telescope Array [47]. The KASCADE [48] results are using a 5 component fit of H, He, CNO, MgSi and Fe groups using Sibyll 2.1. Therefore only the H and He spectra are compared directly as the other groups are strongly correlated. KASCADE-Grande [49] results are using a 3 component fit of H, HeCNO and Heavy groups using Sibyll 2.1. Therefore only the H and Heavy spectra are compared, as the HeCNO group cannot be deconvoluted into a He and CNO part. The Tunka [50] results are using a 4 component fit of H, He, N and Fe groups using QGSJET II-04. The Pierre Auger Observatory [51] results are calculated by using their published elementary group fraction for H, He, N and Fe using Sibyll 2.1 convoluted with their most recent energy spectrum. Note that differences in how different experiments handle intermediate elements (not one of the four groups used here) may lead to some small systematic differences in flux measurements between different experiments.

TALE (TA low-energy extension) ICRC 2017

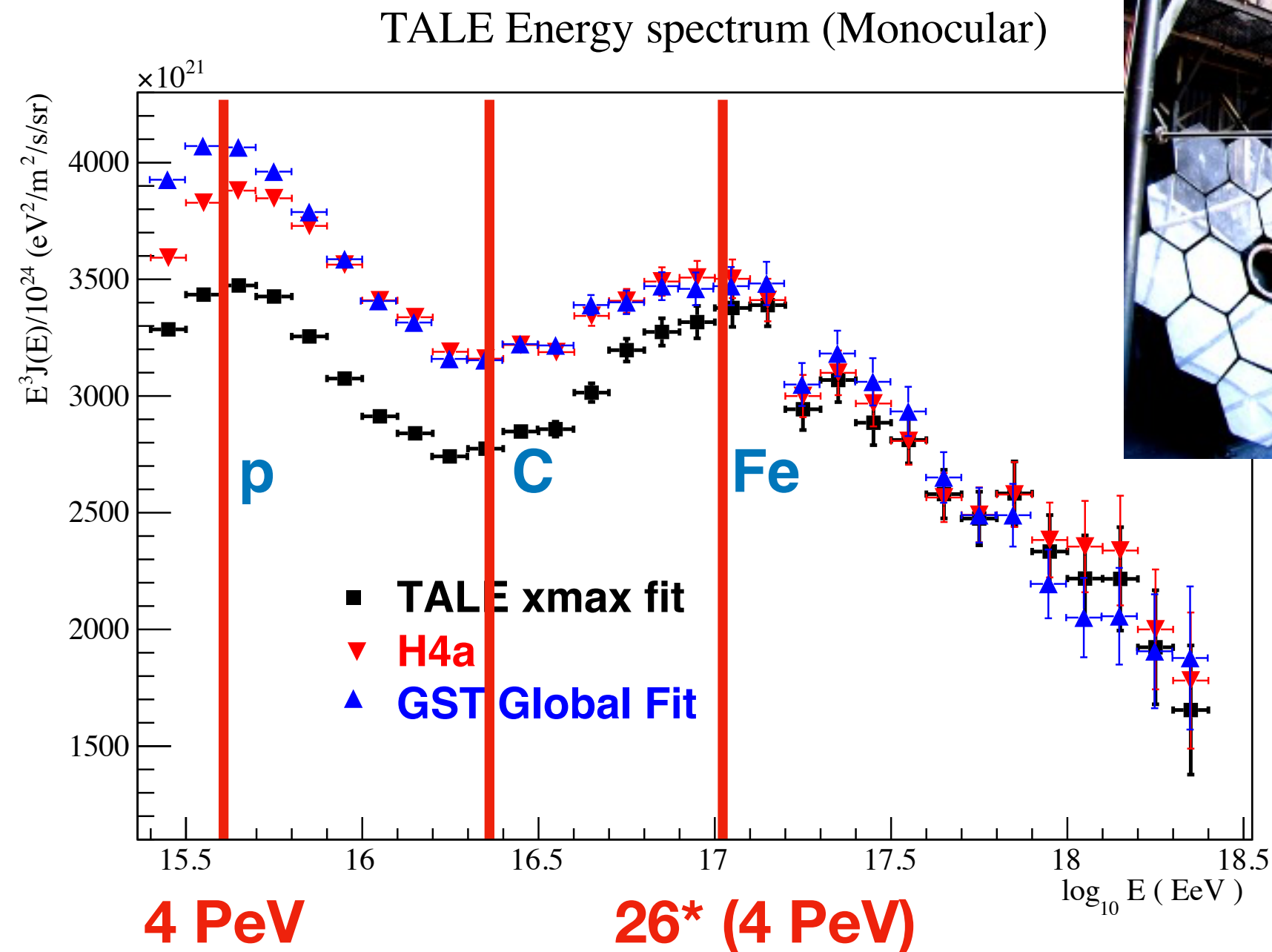
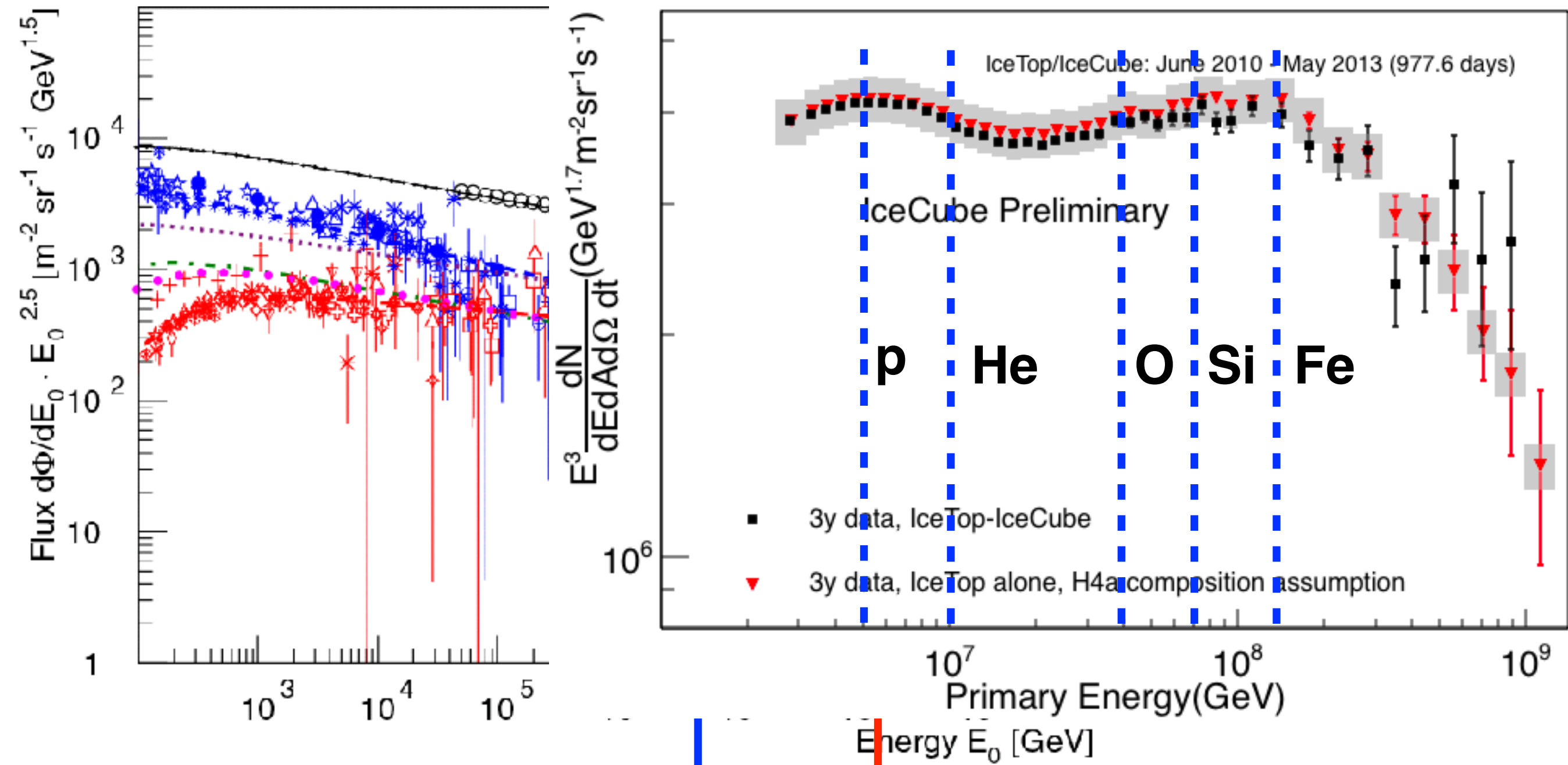


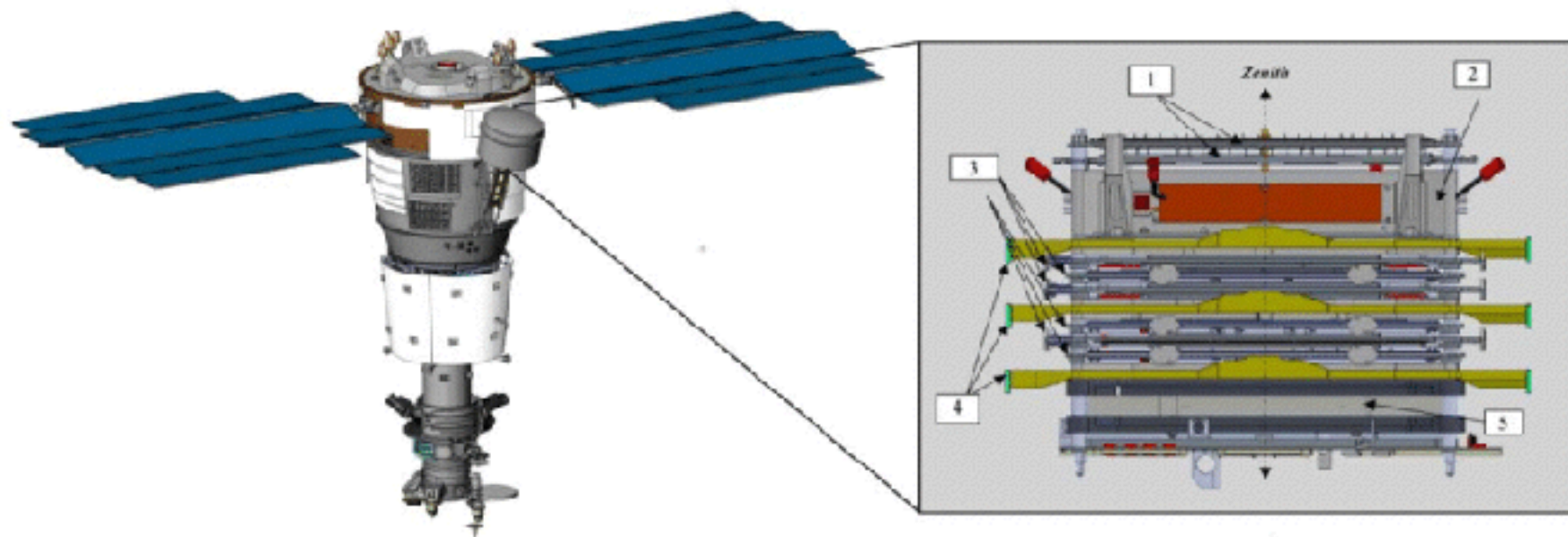
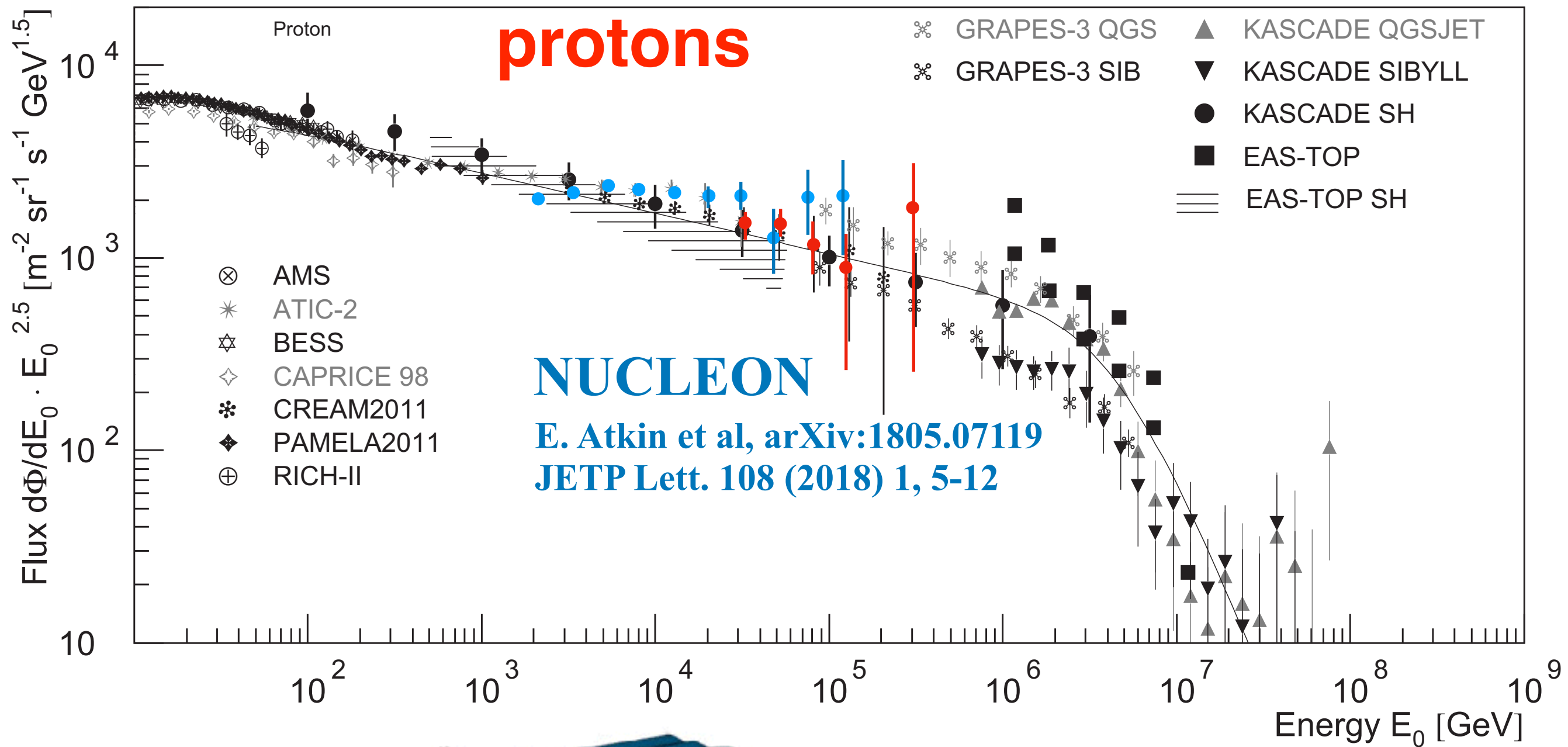
Figure 3: TALE Cosmic rays energy spectrum measured with TALE. The result is based on a QGSJet II-3 hadronic model assumption. A mixed primary composition given by the H4a, and “global fit” models, as well as a TALE derived mix was used in the calculations.

Cosmic-ray energy spectrum





some
remarks



Observation of a knee in the Cosmic Ray p+He energy spectrum below 1 PeV by ARGO-YBJ

A. D'Amone, I. De Mitri, A. Surdo*

*Dipartimento di Matematica e Fisica "E. De Giorgi" - Università del Salento
and Istituto Nazionale di Fisica Nucleare (INFN) - Sezione di Lecce*

Via per Arnesano, I-73100, Lecce, Italy

E-mail: surdo@le.infn.it

for the ARGO-YBJ Collaboration

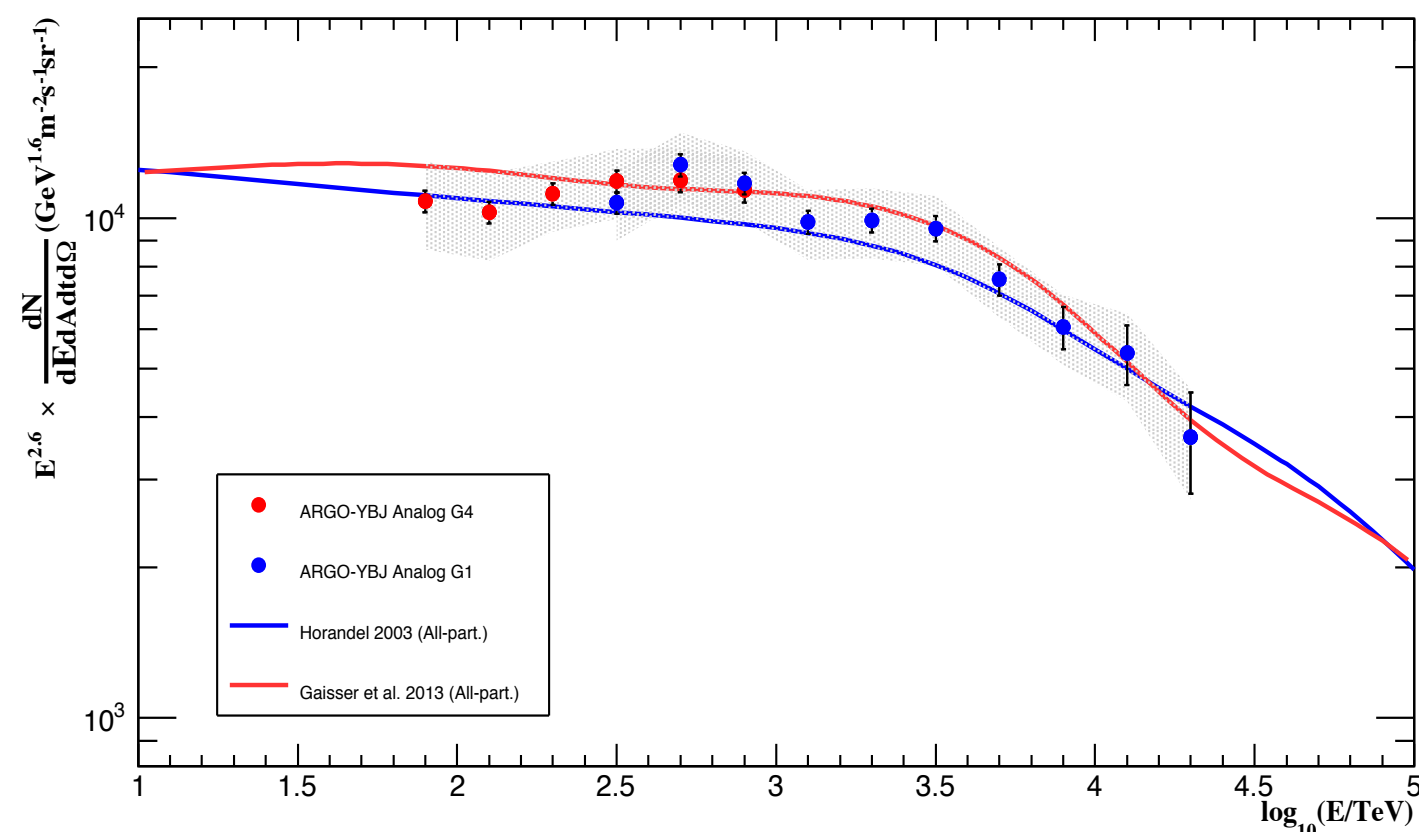


Figure 4: The all-particle energy spectrum of primary CRs resulting from this work. The parametrizations provided by [4] and [23] are shown for comparison.

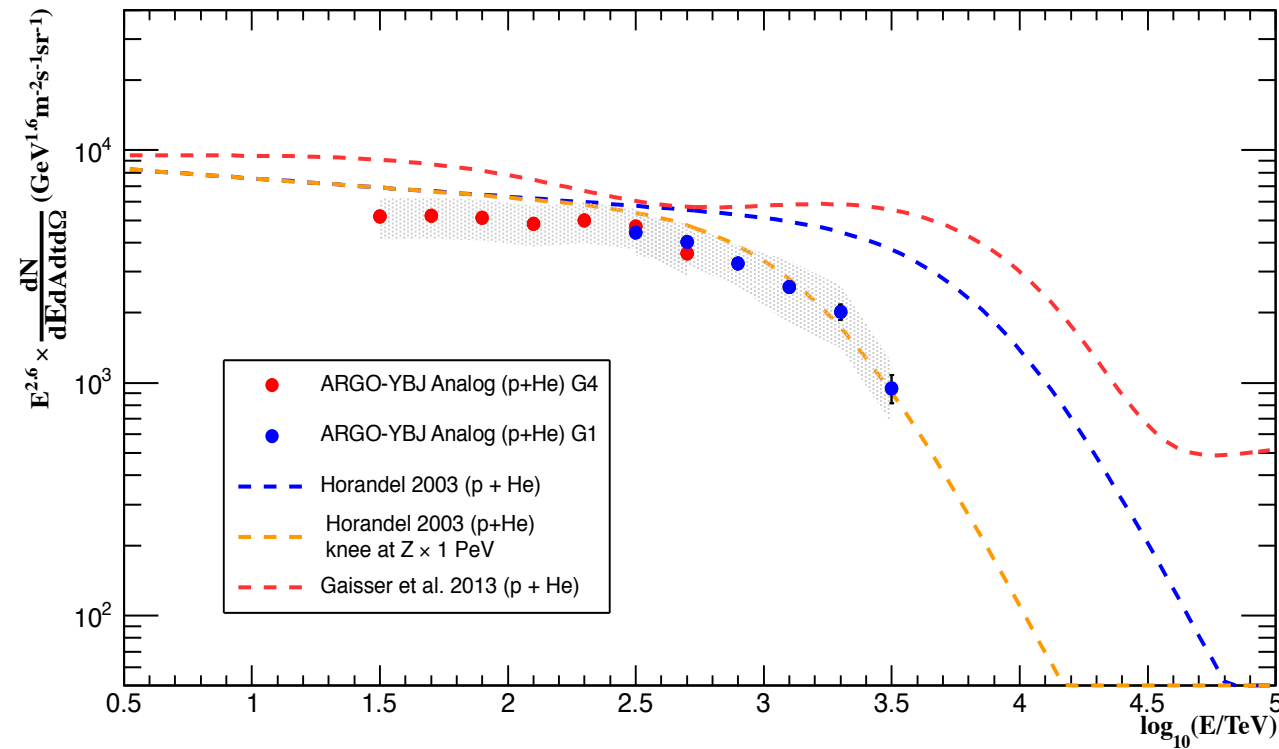


Figure 6: Light (i.e. $p+He$) component energy spectrum of primary CRs as measured in the analysis of ARGO-YBJ analog data (see text).

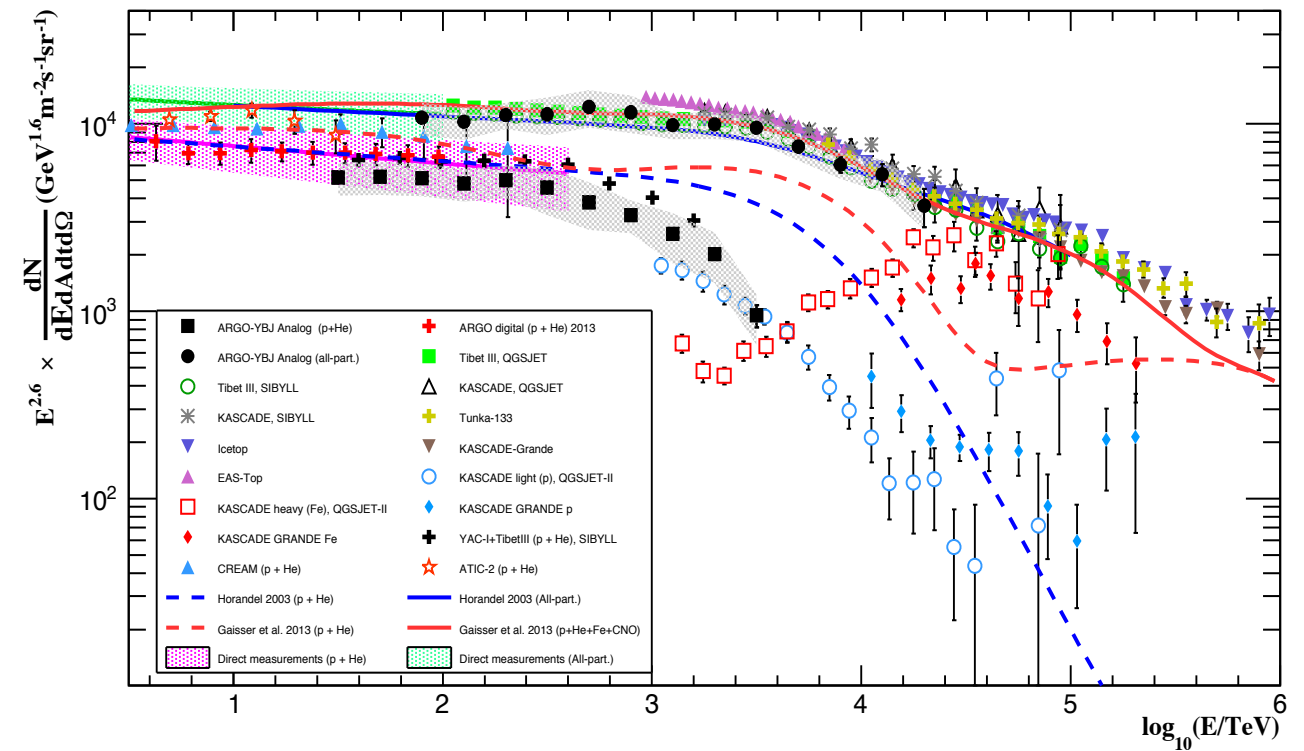


Figure 7: All-particle and light-component energy spectra of primary CRs as measured in this work, compared to several other experimental results.

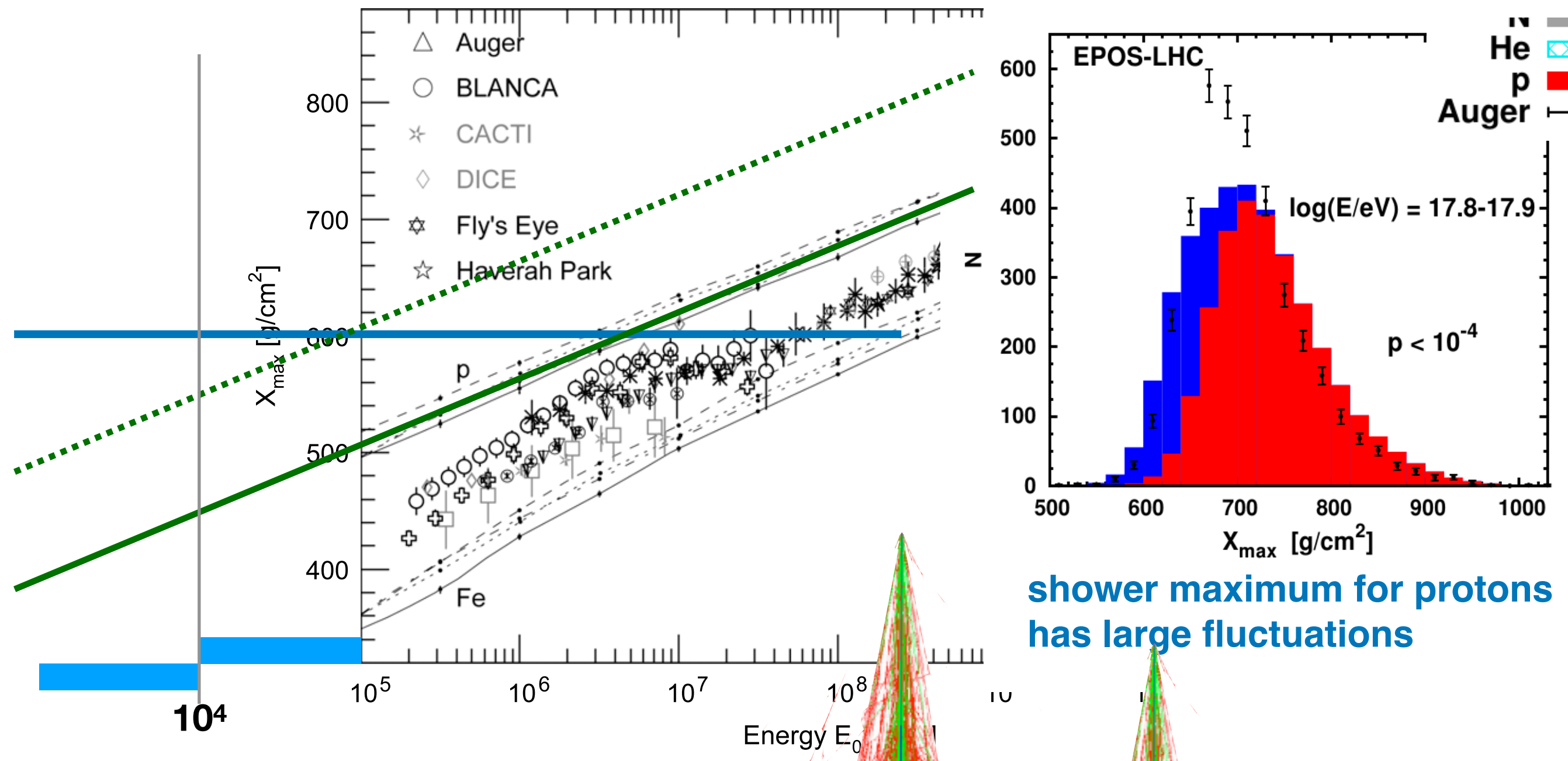
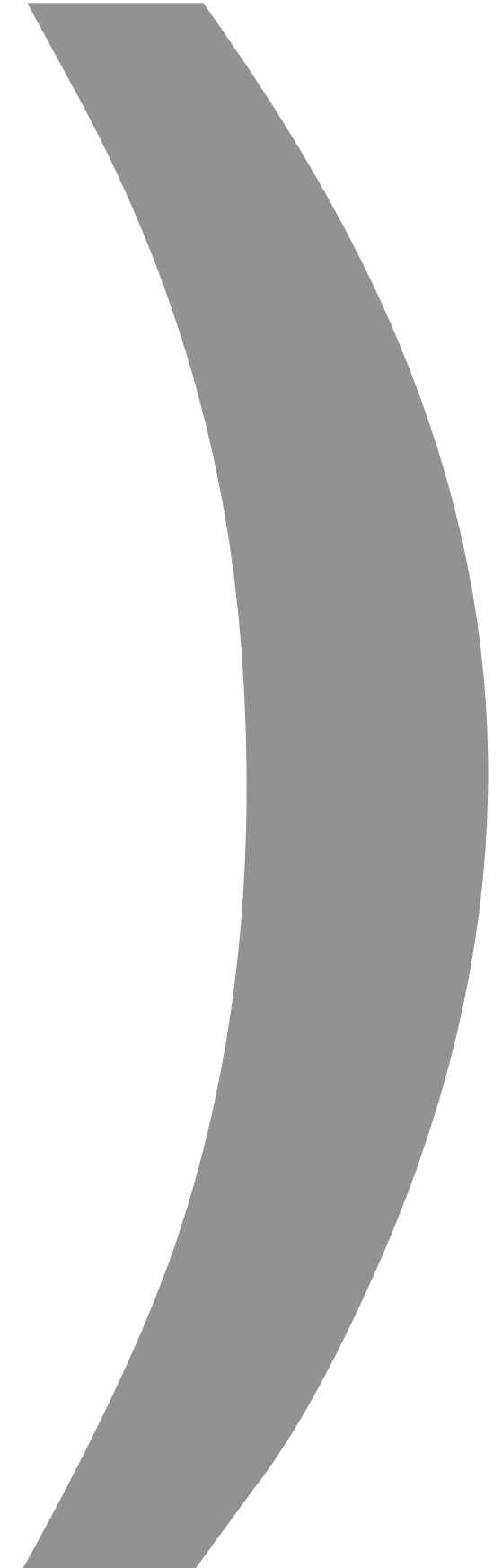


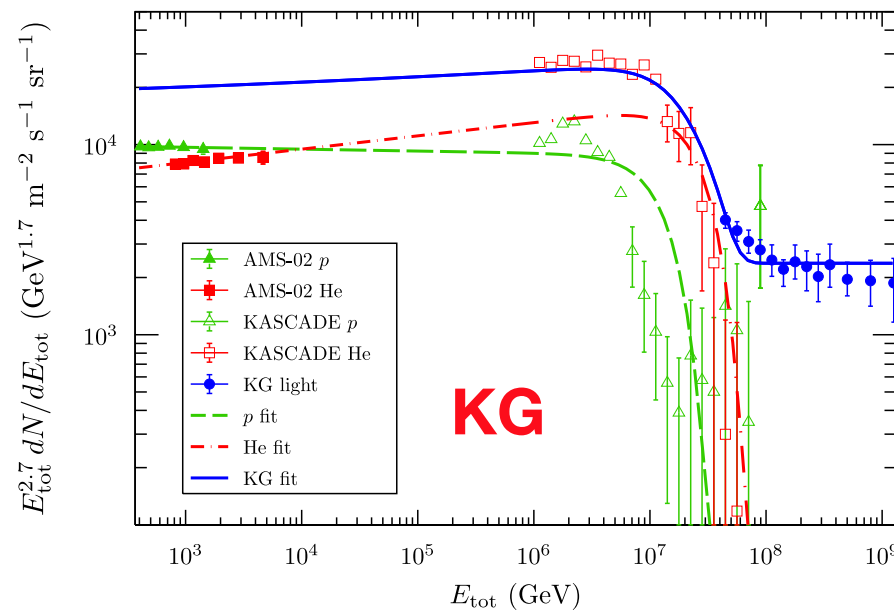
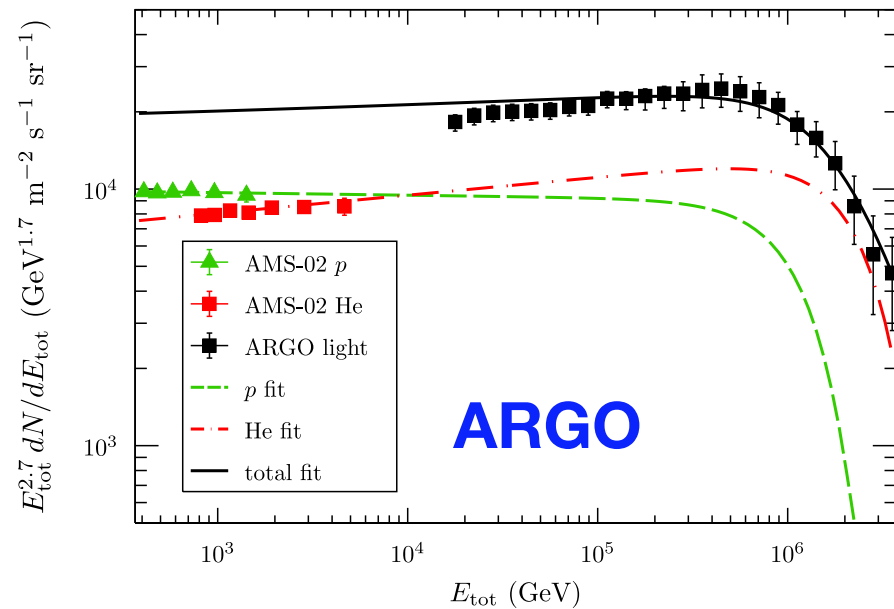
Fig. 13. Average depth of the shower maximum X_{max} as function of primary energy E_0 . Data points are taken from: Auger [30], BLANCA [173], CACTI [306], DICE [182], Fly's Eye [307], Haverah Park [308], HEGRA [174], HiRes/MIA [228], HiRes [309], IceTop [310], SPASE/VULCAN [311], Tunka-25 [176], Yakutsk [312]. The lines indicate simulations for proton and iron induced showers using the CORSIKA model with the hadronic interaction model QGSJET 01 (—), QGSJET II-3 (---), SIBYLL 2.1 (...), and EPOS 1.6 (----).

ARGO at 4300 m.a.s.l. = 606 g/cm²

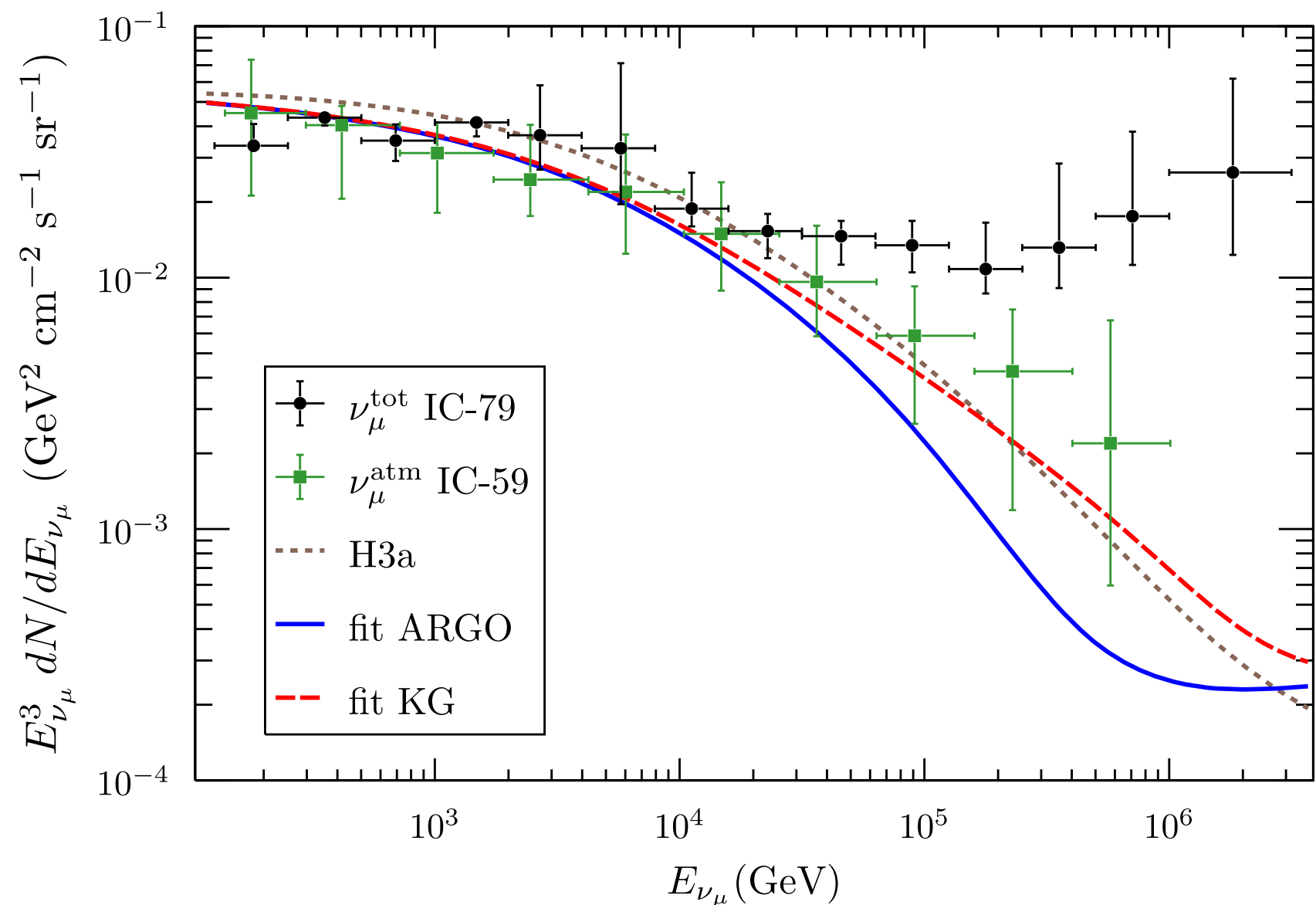
some
remarks

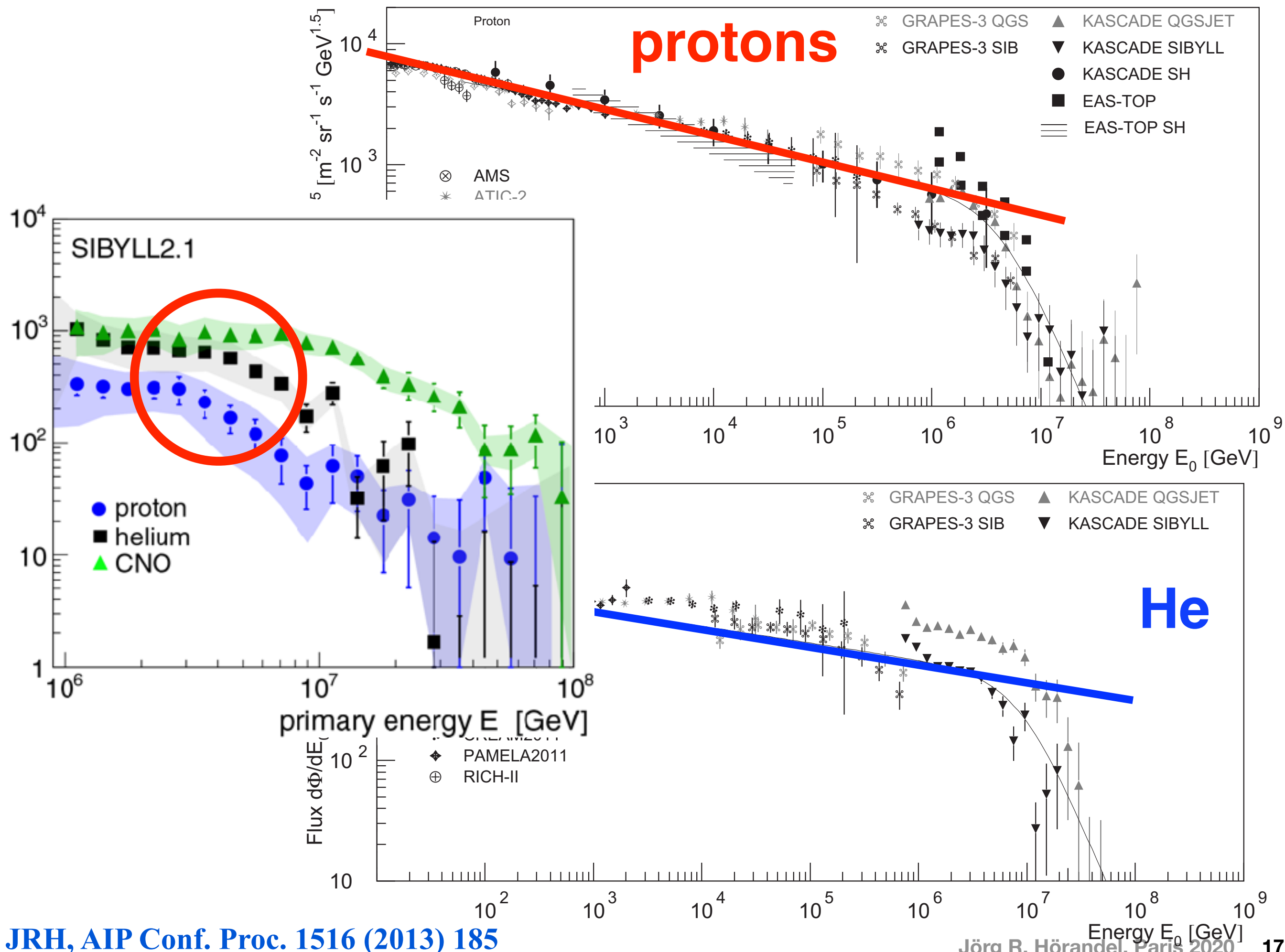


Atmospheric neutrinos and the knee of the cosmic ray spectrum



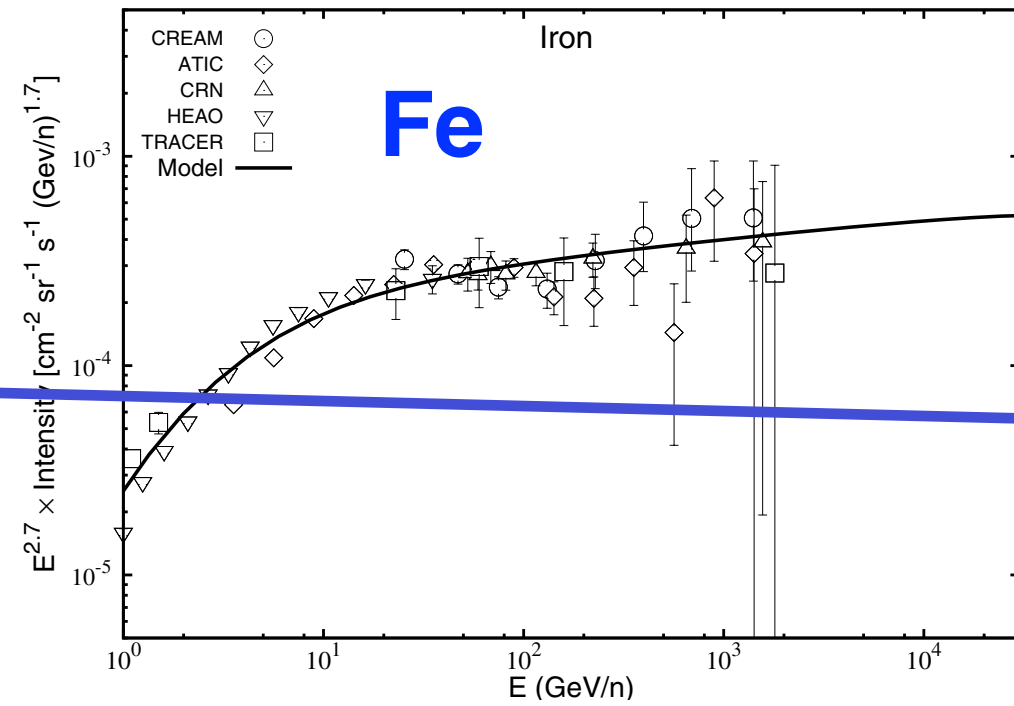
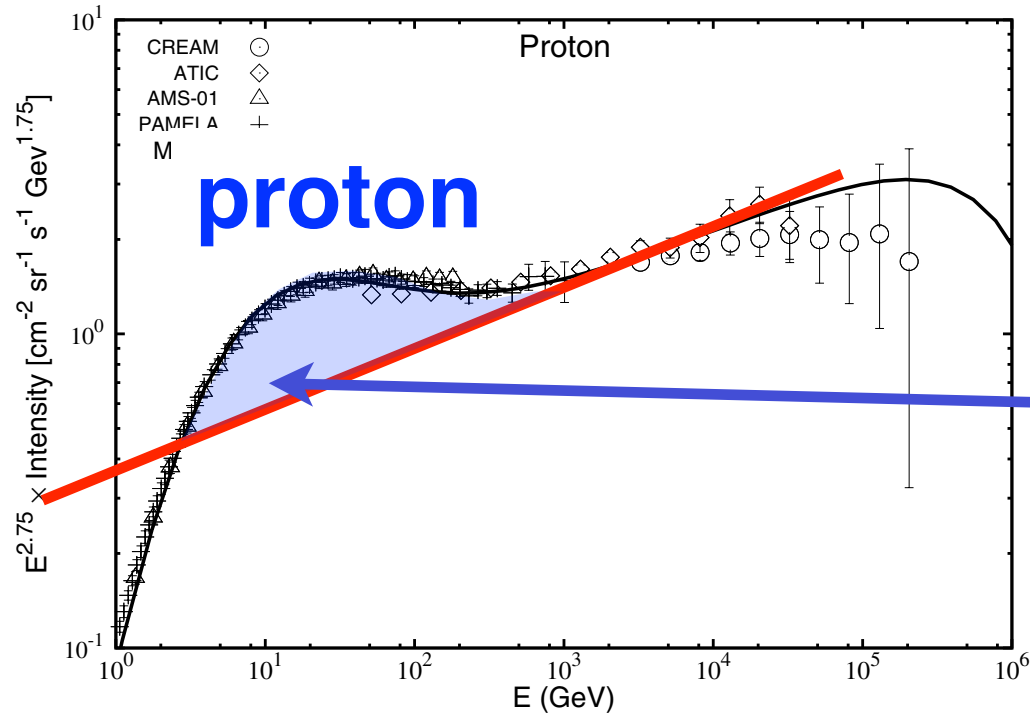
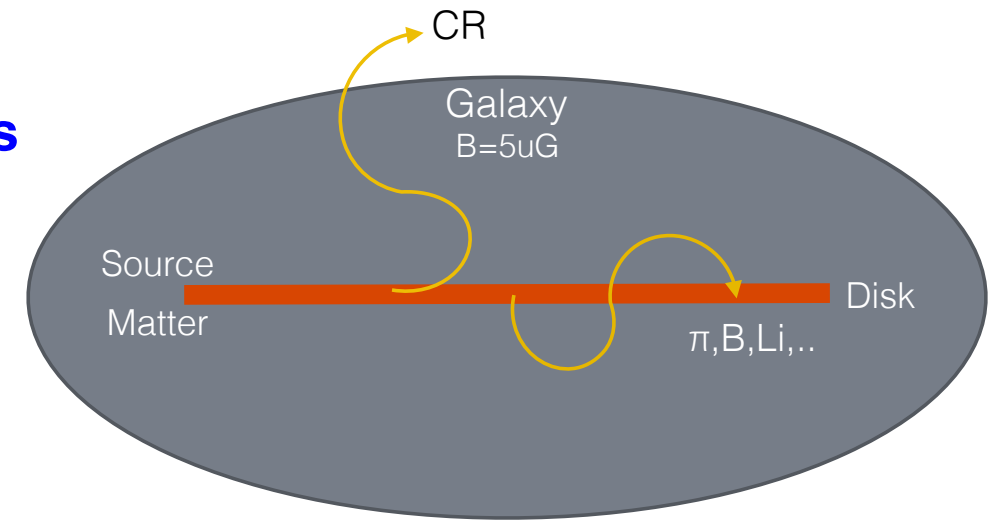
take ARGO + KASCADE-Grande measurements to predict neutrino flux



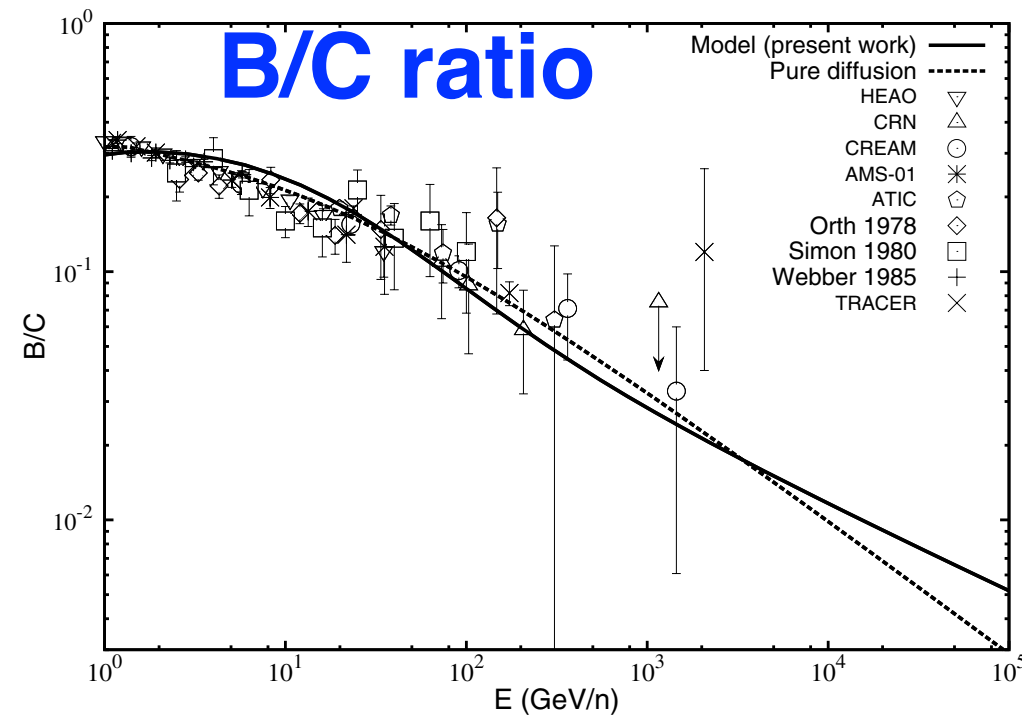
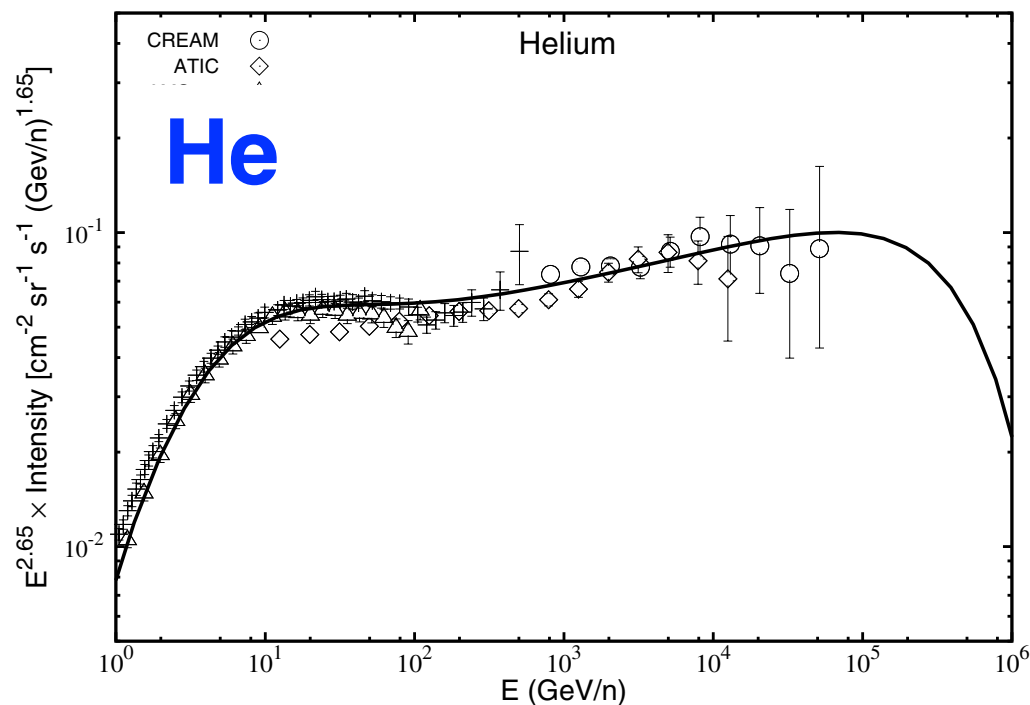


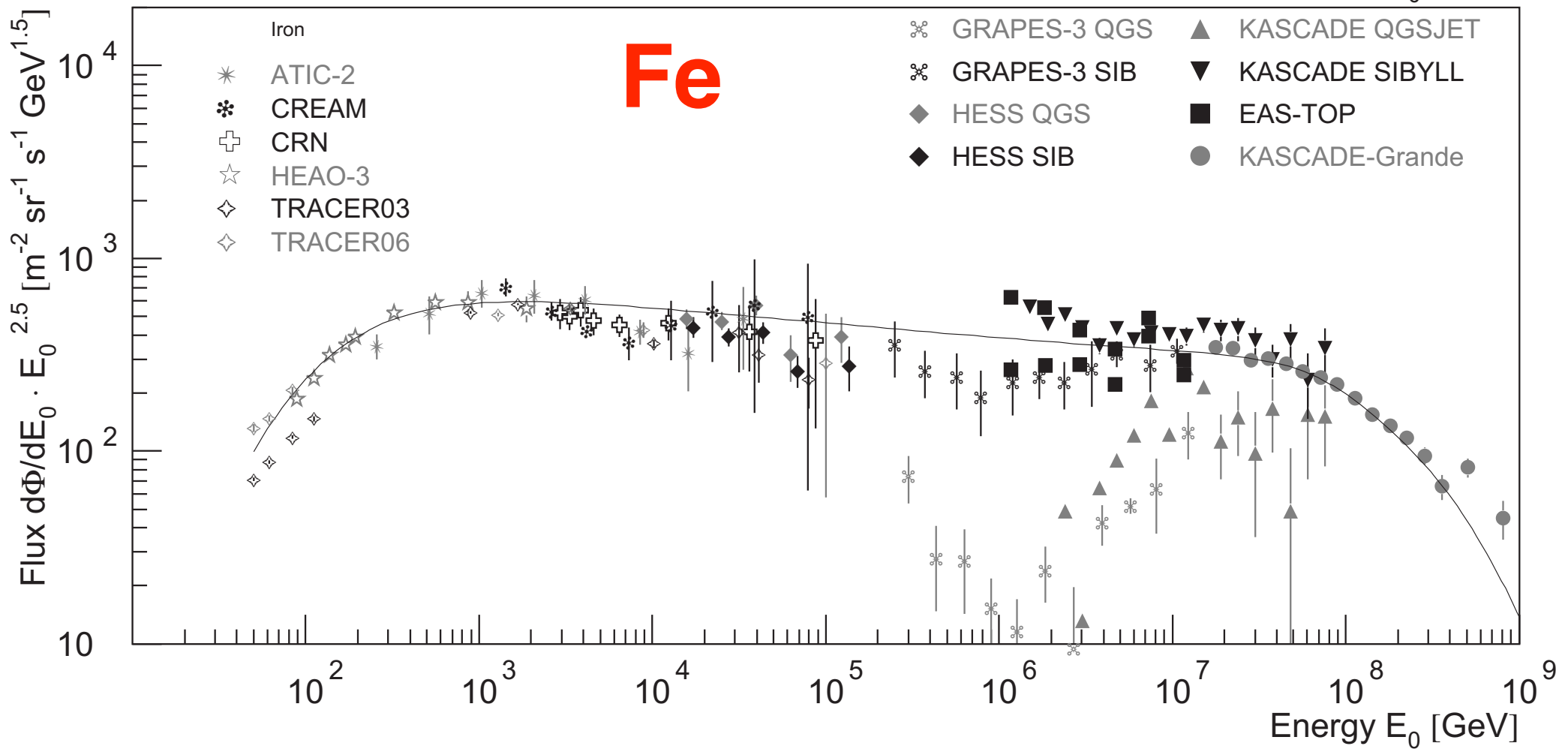
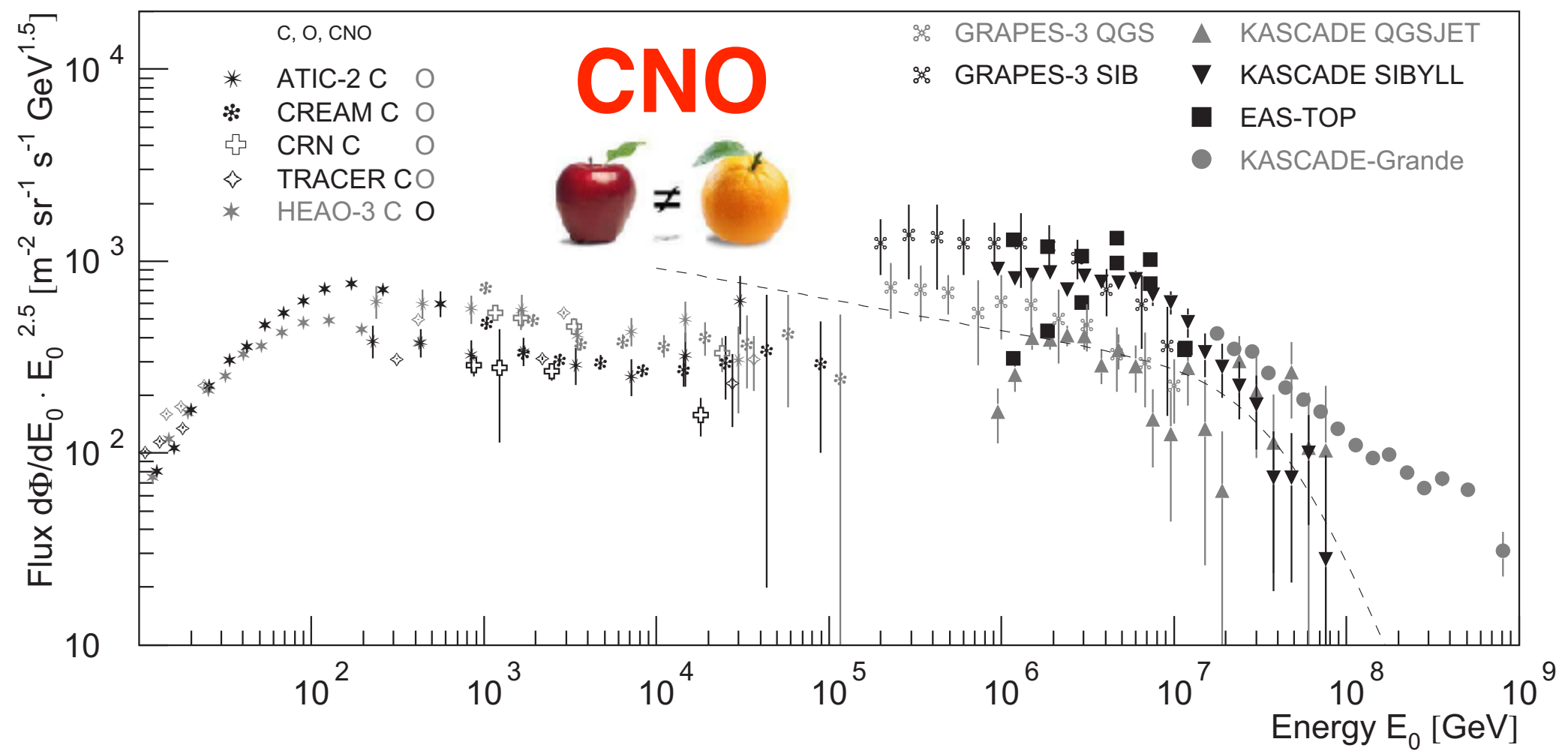
GeV-TeV cosmic-ray spectral anomaly as due to reacceleration by weak shocks in the Galaxy★

Satyendra Thoudam and Jörg R. Hörandel



bump due to reacceleration by weak shocks in the Galaxy





Origin of the knee? JRH, Astropart. Phys. 21 (2004) 241 (updated)

Acceleration (SNR)

- .. in SNR
- .. in SNR + radio galaxies
- .. in oblique shocks
- .. in variety of SNR
- Single source model
- Reacceleration in galactic wind

Leakage from Galaxy

- Minimum pathlength model
- Anomalous diffusion model
- Hall diffusion model
- Diffusion in turbulent magnetic fields
- Diffusion and drift

γ -ray bursts

- Cannonball model
- Acceleration in GRB + diffusion
- Acceleration in GRB $E_{\max} \sim A$

Interaction with background particles

- Diffusion model + photo-disintegration
- Interaction with neutrinos in galactic halo
- Photo-disintegration (optical and UV photons)

Particle physics in atmosphere

- Gravitons, SUSY

Berezhko & Ksenofontov

Stanev ..

Kobayakawa ..

Sveshnikova

Erlykin & Wolfendale

Völk & Zirakashvili

Swordy

Lagutin ..

Ptuskin .., Kalmykov ..

Ogio & Kakimoto

Roulet ..

Plaga

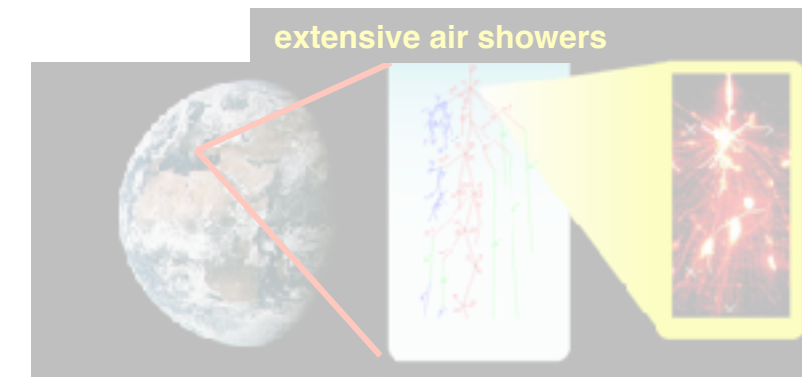
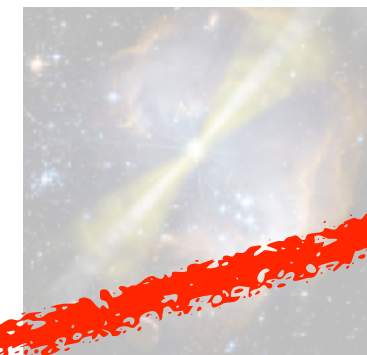
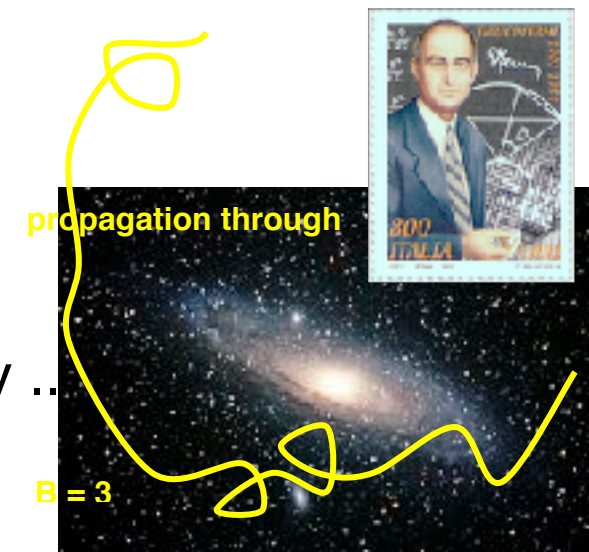
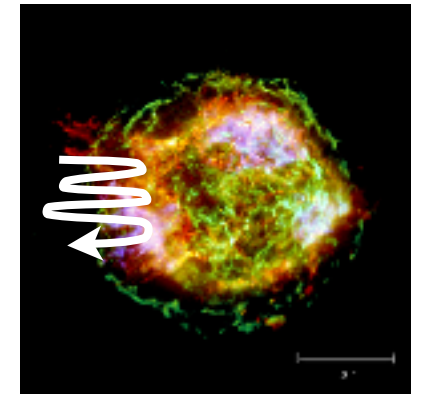
Wick ..

Dar ..

Dova ..

Candia ..

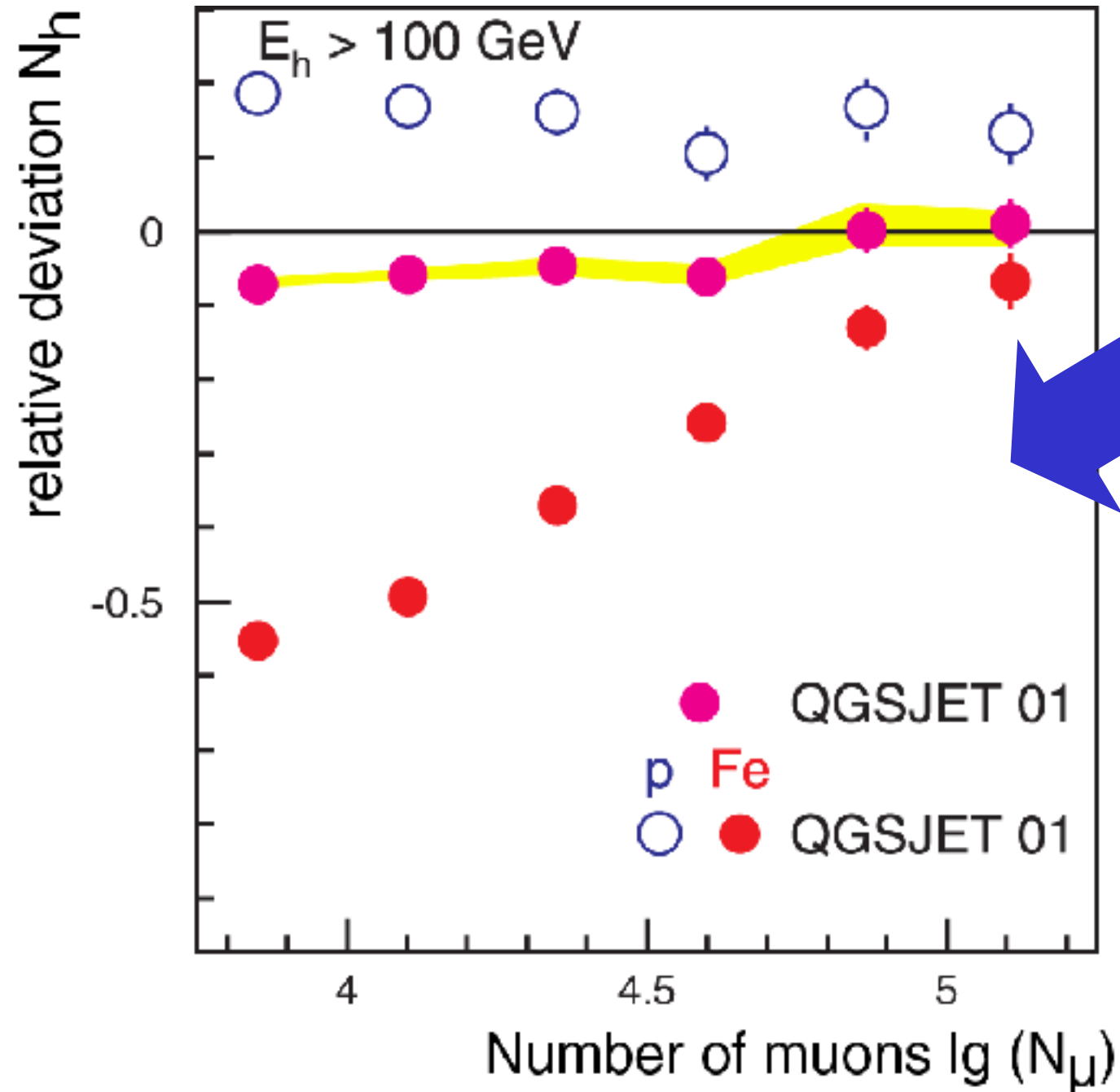
Kazanas & Nicolaidis



Test of hadronic interaction models

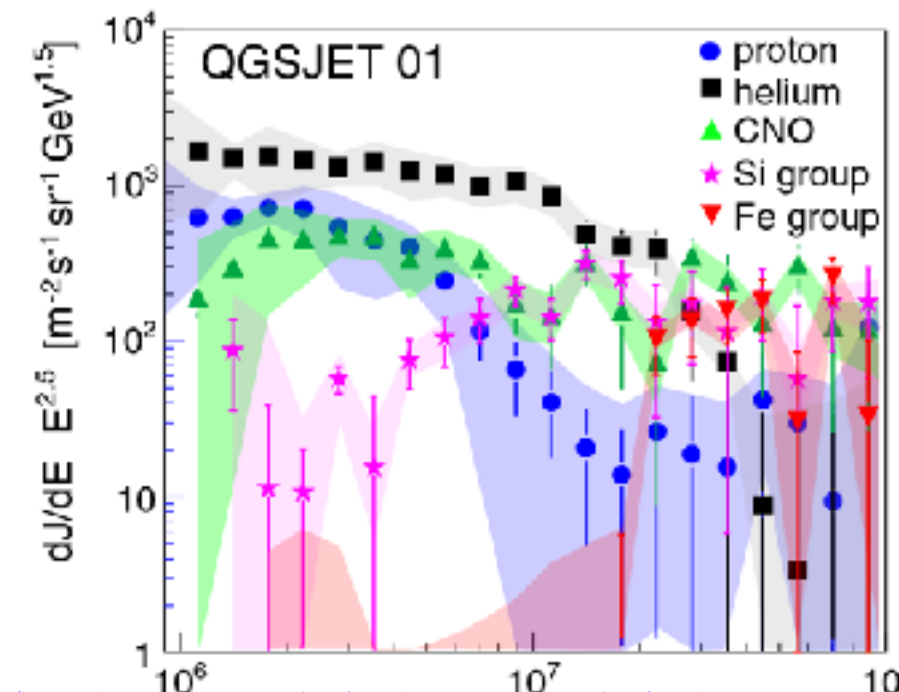
QGSJET 01

Number of hadrons vs. number of muons



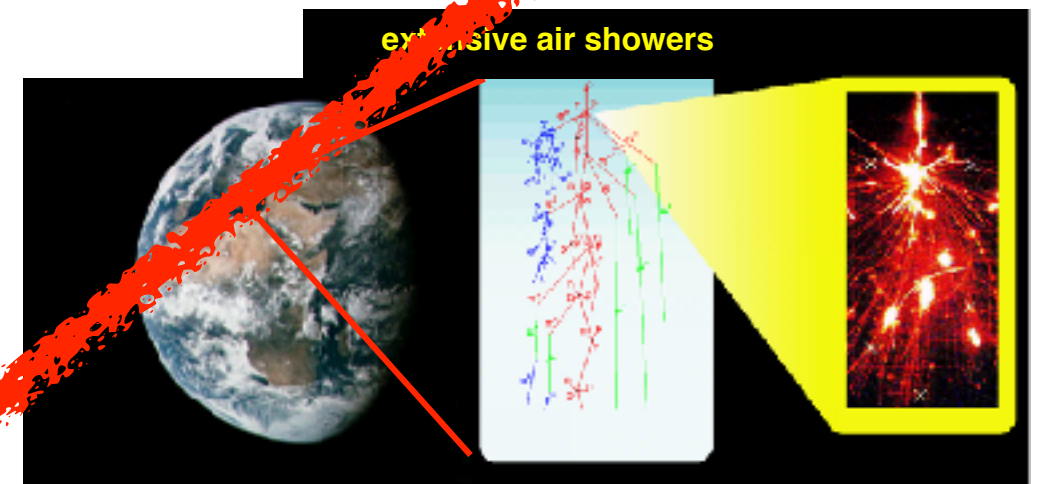
inconsistencies on 10% level

N_e - N_μ analysis



in literature:

ideas that knee is caused by new interactions in atmosphere
—> energy is carried away by „invisible channels“



Electron, muon and hadron size spectra of EAS in the "knee" region

R. Glasstetter^a and J.R. Hörandel^a for the KASCADE Collaboration*

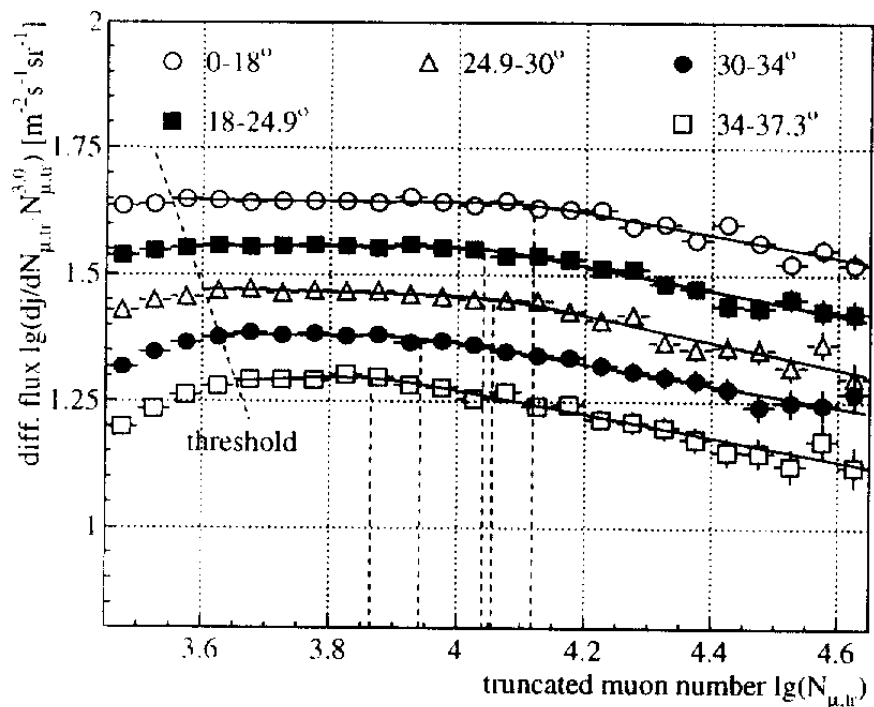
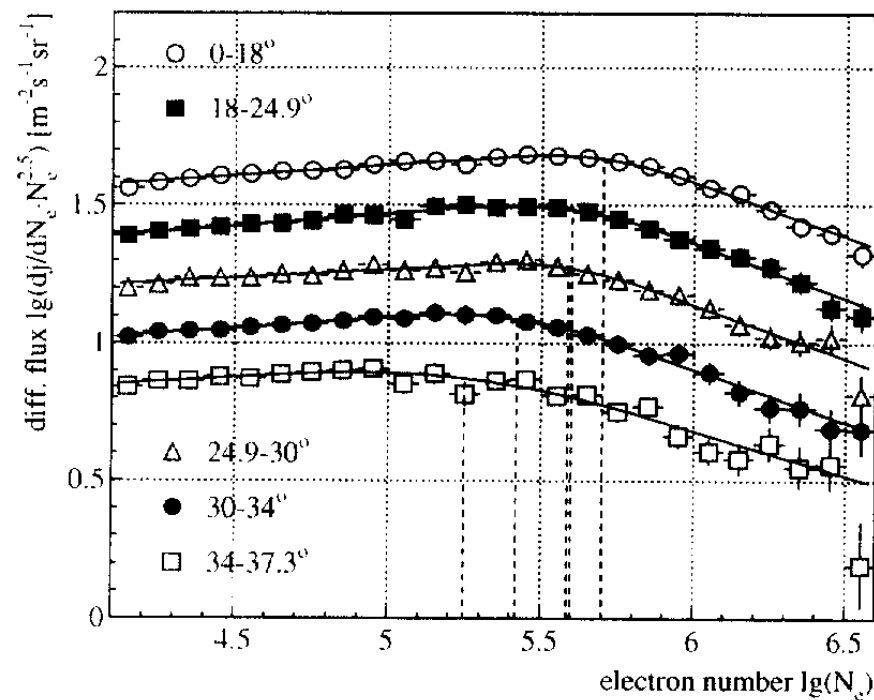


Figure 1. Electromagnetic (top) and muonic (bottom) shower size spectra for different zenith angle bins.

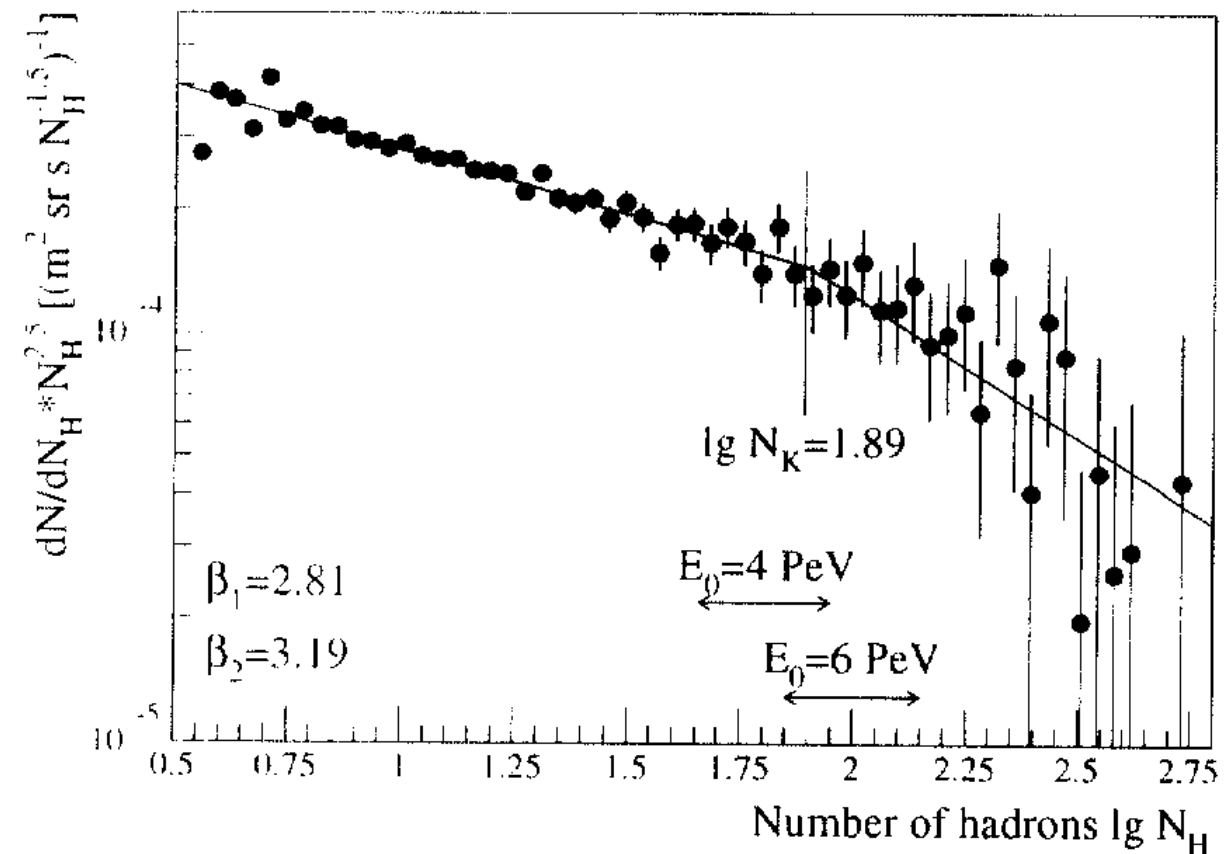


Figure 3. Hadronic shower size spectrum.

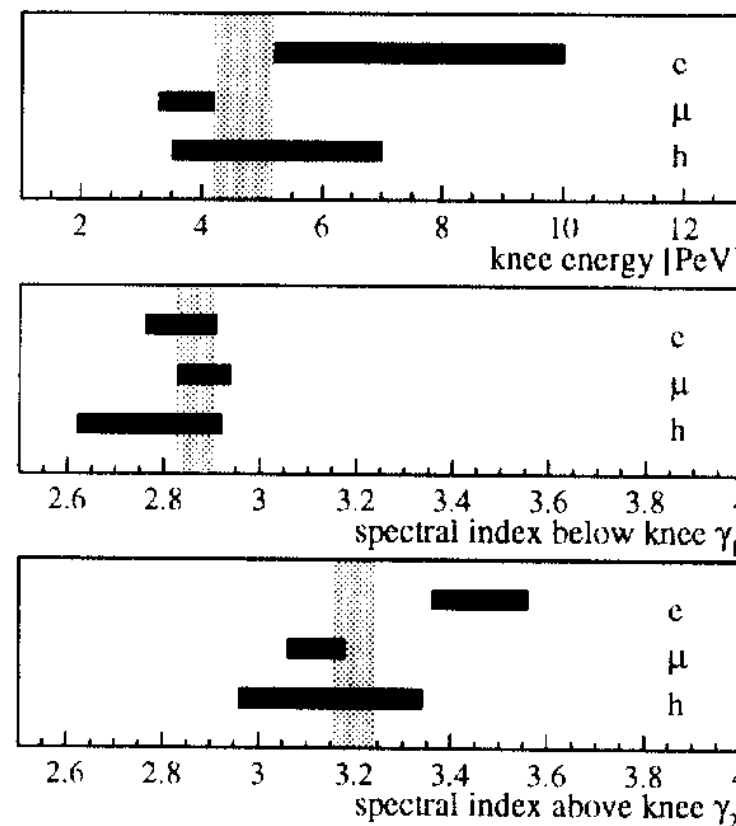
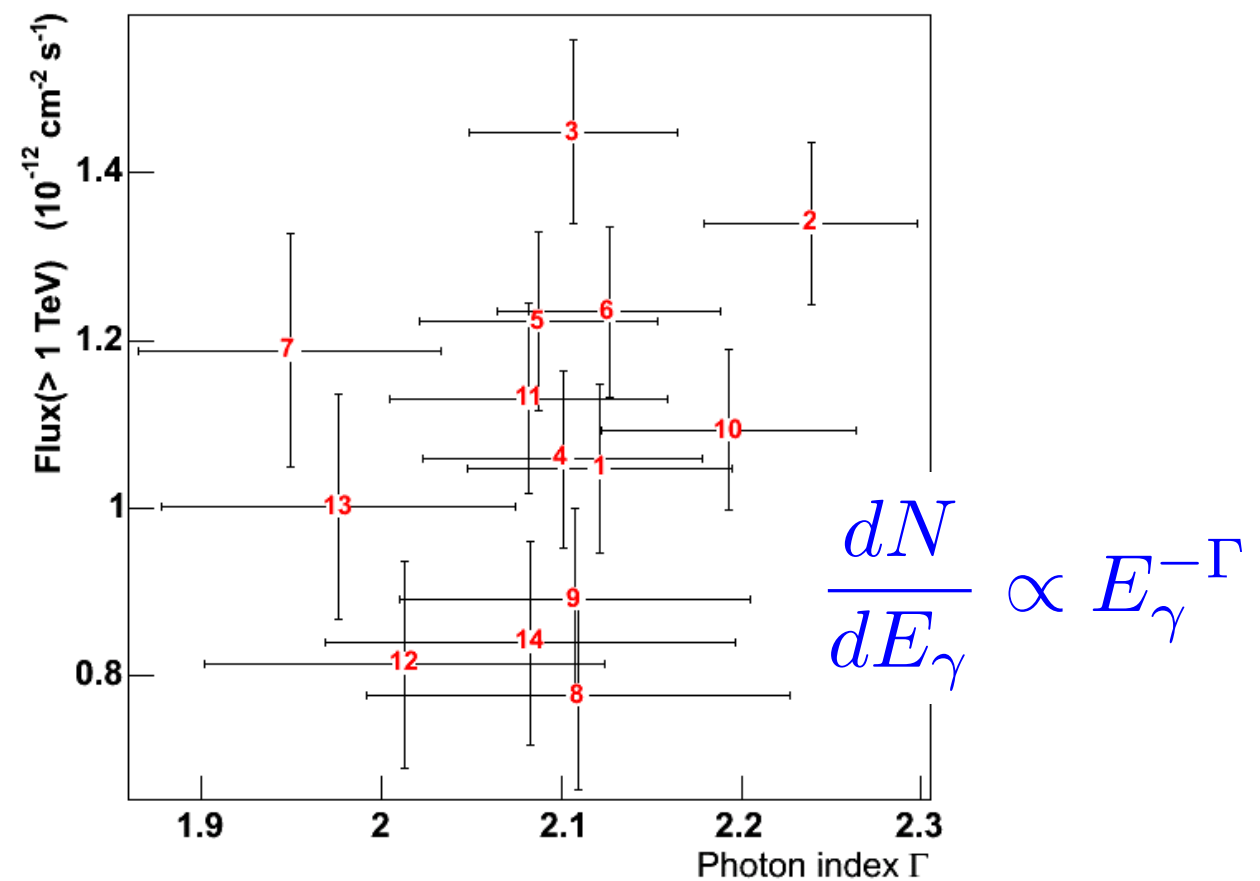
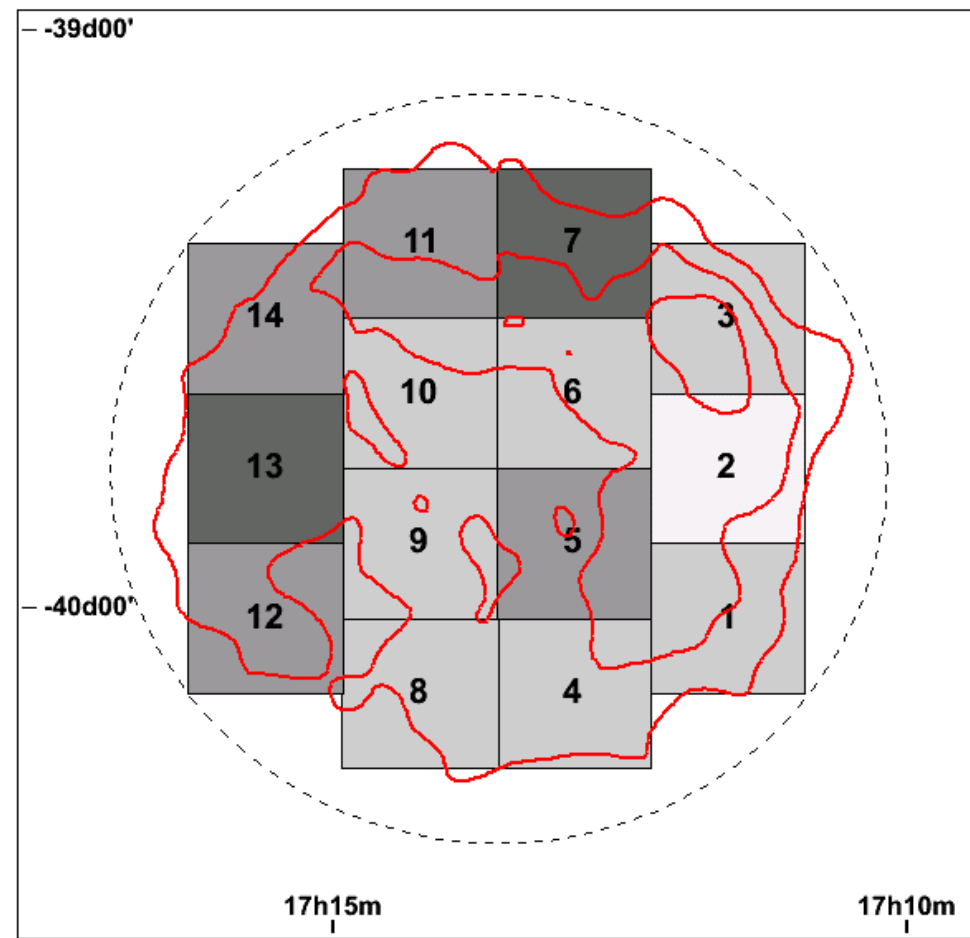
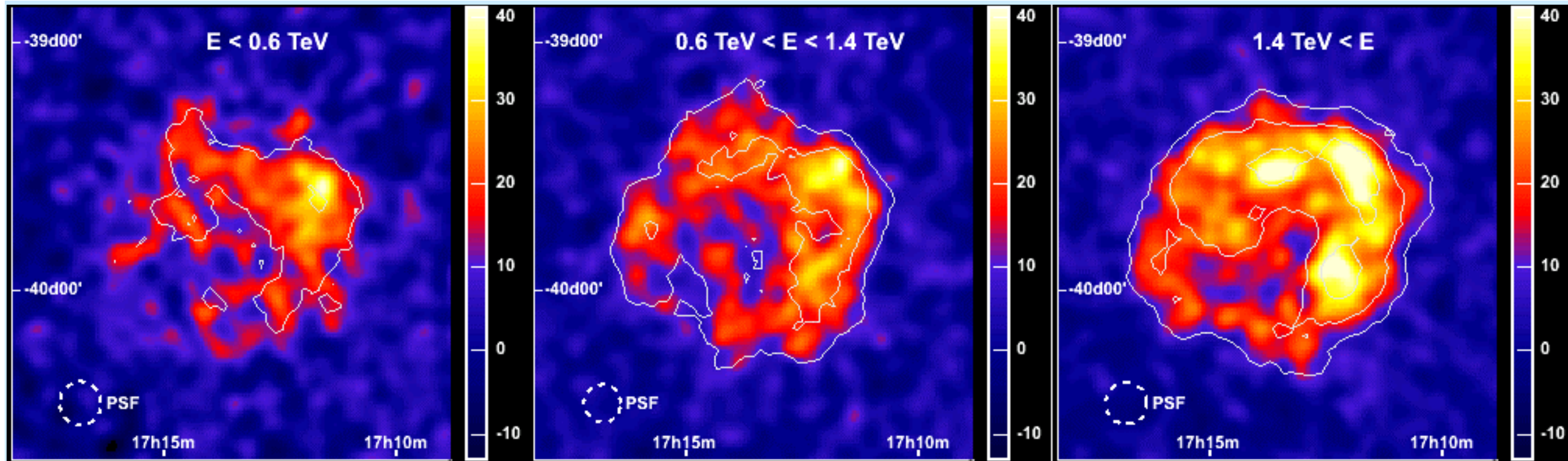


Figure 4. Knee position and spectral indices.

*knee observed in
all components,
electromagnetic,
muonic, and
hadronic!*

H.E.S.S. supernova remnant RXJ 1713



Acceleration of cosmic rays at SNR

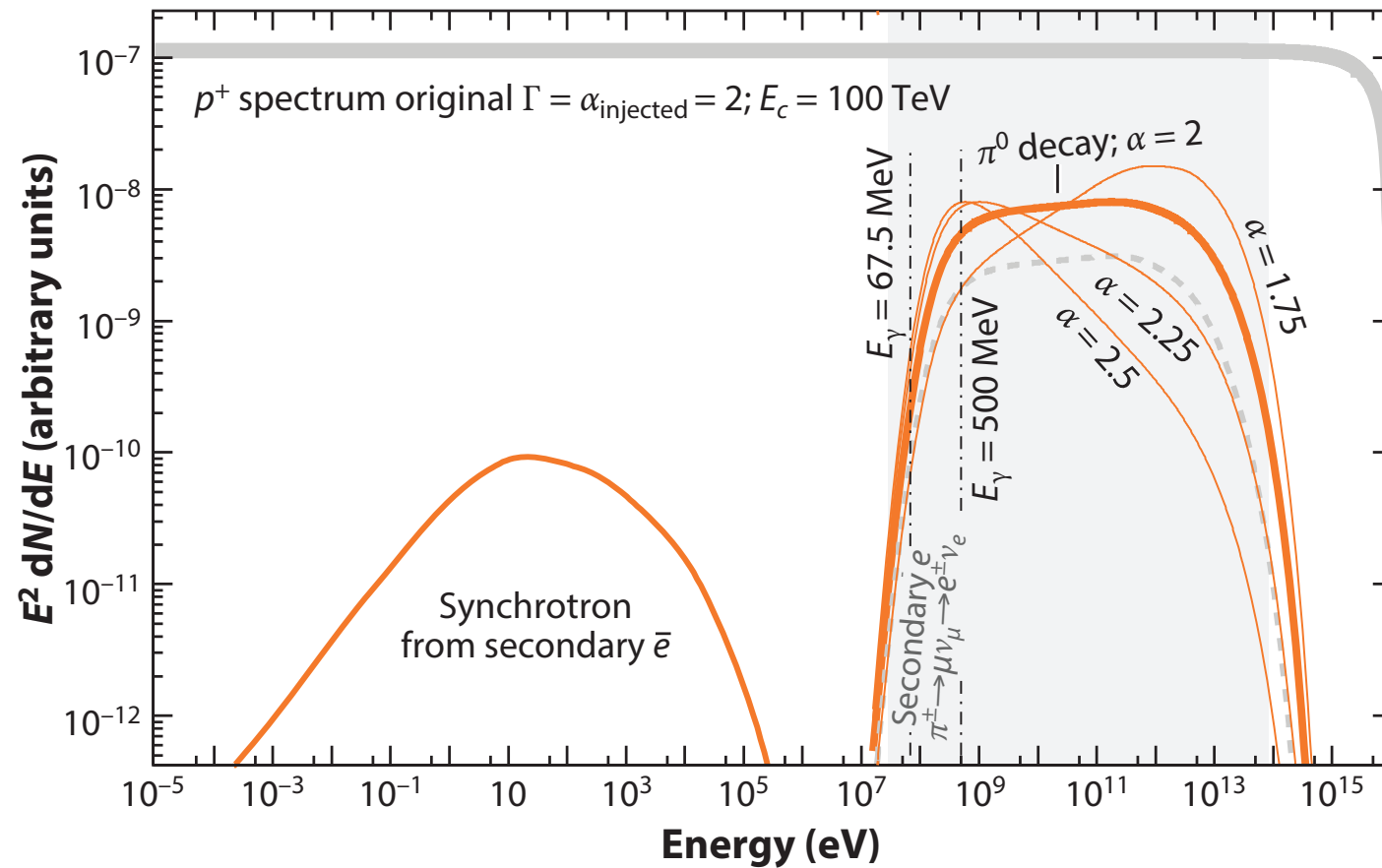


Figure 3

Spectral energy distribution of accelerated protons (power-law index $\alpha_{\text{injected}} = 2.0$ and cutoff at 100 TeV) and γ -rays resulting from inelastic collisions with interstellar material. The dominant emission into photons occurs via the decay $\pi^0 \rightarrow \gamma\gamma$ (solid orange curves). The γ -ray spectrum follows the parent protons' spectrum rather closely in the midenergy range and in the high-energy cutoff region. For all proton indices, the low-energy turnover is a characteristic feature of the pion-decay emission. Also shown is the spectrum of electrons resulting from the inelastic proton-proton interactions via the decay chain $\pi^\pm \rightarrow \mu + \nu_\mu \rightarrow e^\pm \nu_e$ (dashed gray curve). For the synchrotron emission from these so-called secondary electrons, a source with age $t_{\text{age}} = 1,000$ years and $B = 30 \mu\text{G}$ have been assumed. The shaded gray region shows the sensitive range of current γ -ray detectors (*Fermi*-LAT, imaging atmospheric Cherenkov detectors).

flux at Earth by an astrophysical accelerator that puts a fraction ϵ_{CR} of the energy output into the acceleration of protons:

$$F_\gamma(>100 \text{ MeV}) = 4.4 \times 10^{-7} \epsilon_{\text{CR}} \frac{E_{\text{pr}}}{d^2} \text{ erg cm}^{-2} \text{ s}^{-1}$$

In other words, if the distance d and the density of the interaction region n are known, the number of energy in protons E_{pr} at the interaction site can be directly inferred from the γ -ray flux F_γ .

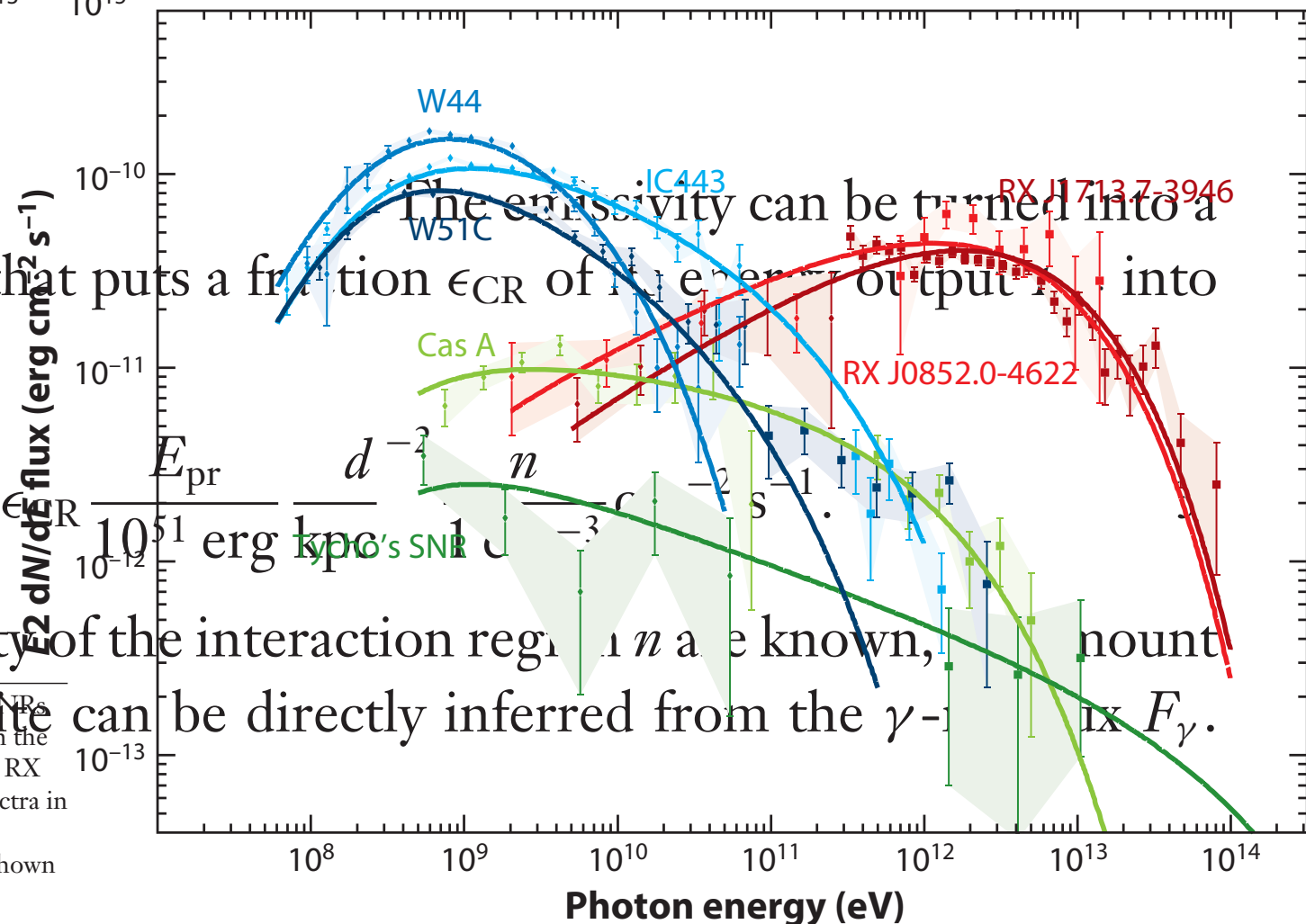


Figure 6

Typical γ -ray energy spectra for several of the most prominent supernova remnants (SNRs). Young SNRs ($<1,000$ years) are shown in green. These typically show smaller γ -ray fluxes but rather hard spectra in the GeV and TeV bands. The older (but still referred to as young) shell-type SNRs RX J1713.7-3946 and RX J0852.0-4622 (Vela Junior) of ages $\sim 2,000$ years are shown in shades of red. These show very hard spectra in the GeV band ($\Gamma = 1.5$) and a peak in the TeV band with an exponential cutoff beyond 10 TeV. The middle-aged SNRs ($\sim 20,000$ years) interacting with molecular clouds (W44, W51C, and IC443) are shown in blue. Also shown are hadronic fits to the data (solid lines).

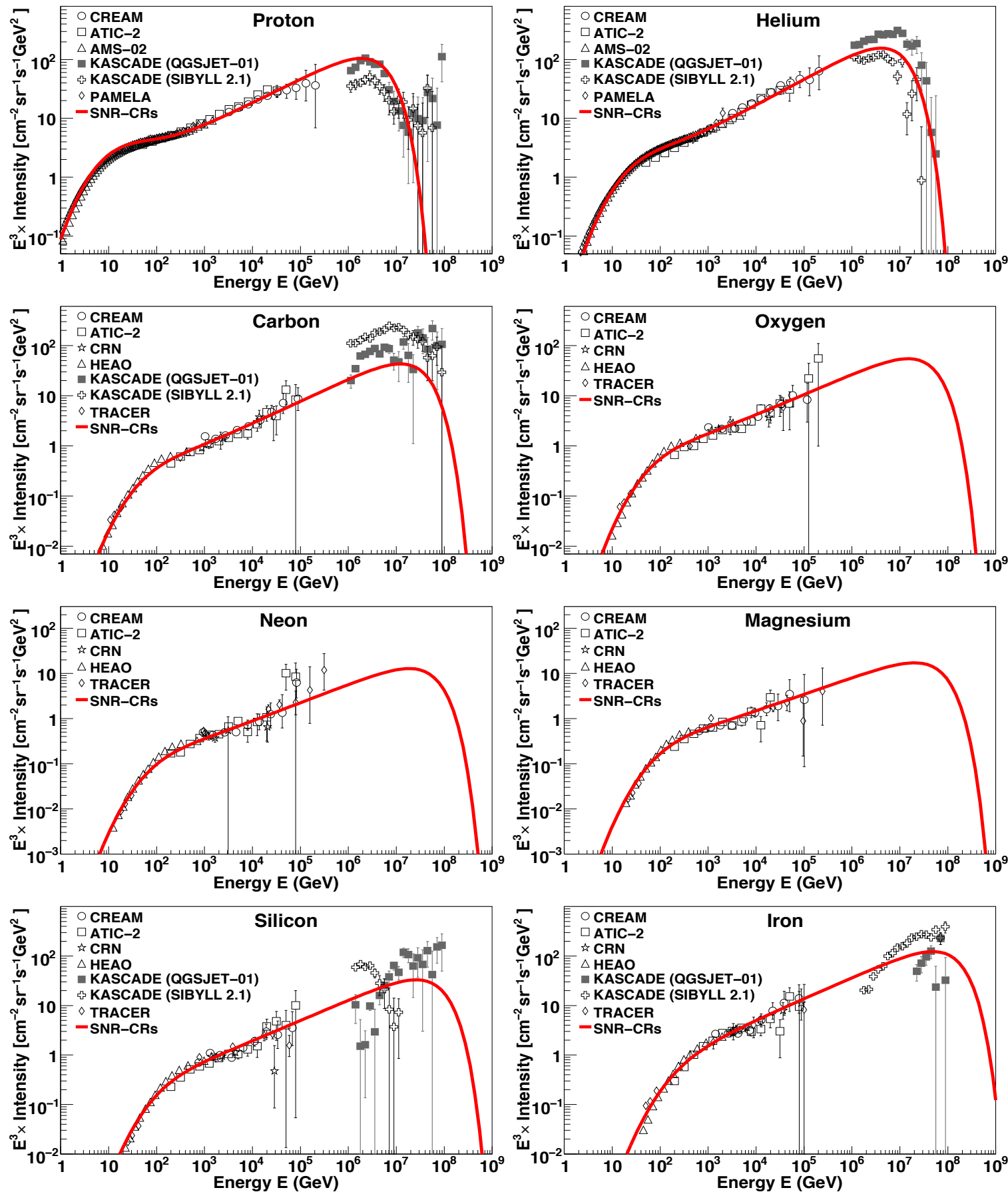


Fig. 1. Energy spectra for different cosmic-ray elements. *Solid line:* Model prediction for the SNR-CRs. *Data:* CREAM (Ahn et al. 2009; Yoon et al. 2011), ATIC-2 (Panov et al. 2007), AMS-02 (Aguilar et al. 2015a,b), PAMELA (Adriani et al. 2011), CRN (Müller et al. 1991; Swordy et al. 1990), HEAO (Engelmann et al. 1990), TRACER (Obermeier et al. 2011), and KASCADE (Antoni et al. 2005). Cosmic-ray source parameters (q, f) used in the calculation are given in Table 1. For the other model parameters (D_0, a, η, s), see text for details.

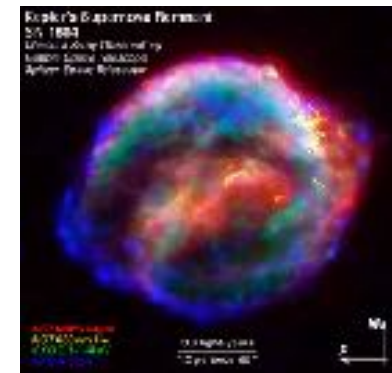
Contribution of (regular) SNR-CR

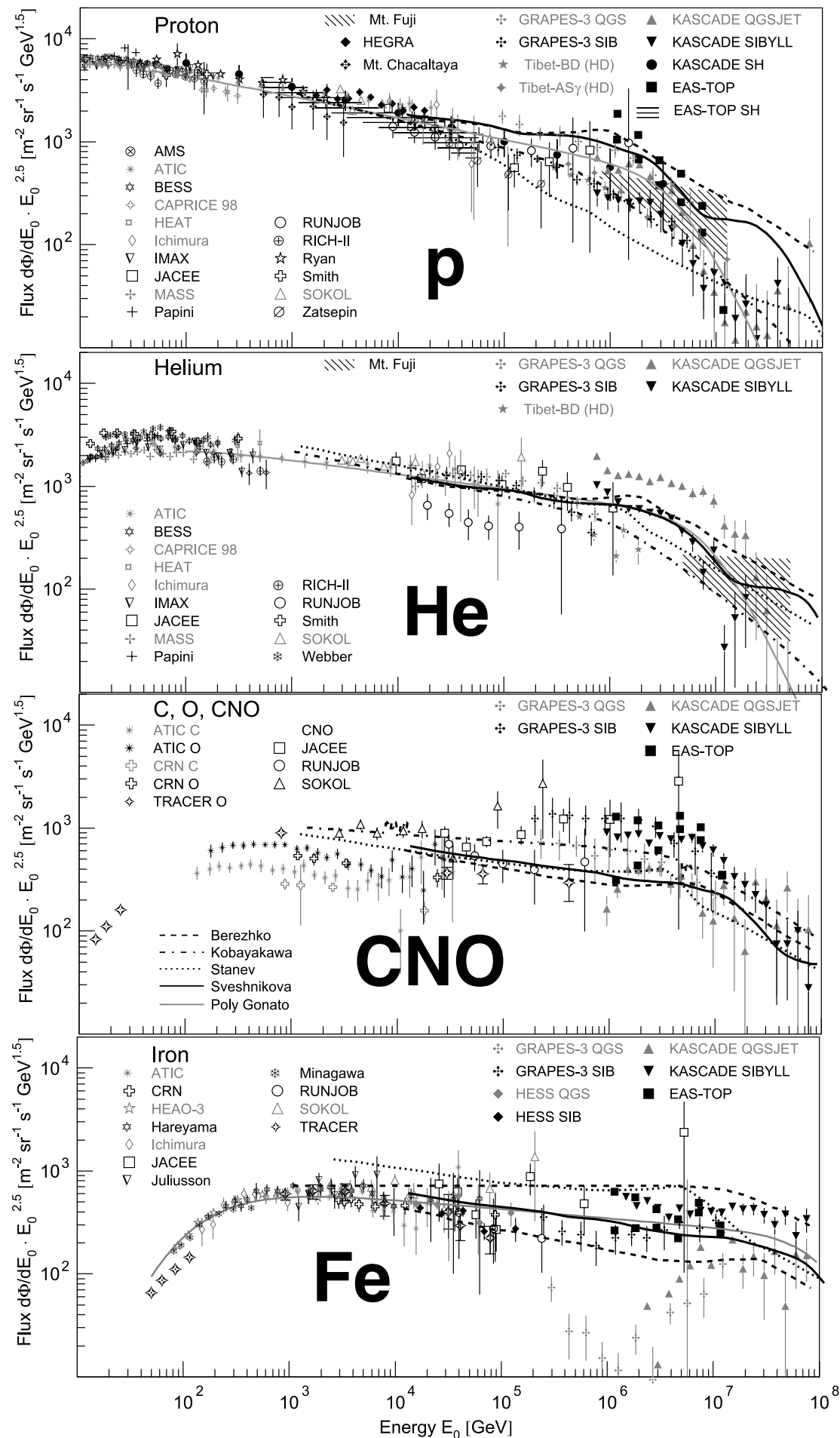
$$E_c = Z \cdot 4.5 \cdot 10^6 \text{ GeV}$$

$$Q(p) = A Q_0 (A p)^{-q} \exp \left(-\frac{A p}{Z p_c} \right),$$

Table 1. Source spectral indices, q , and energy injected per supernova, f , for the different species of cosmic rays used in the calculation of the SNR-CRs spectra shown in Figures 1 and 2.

Particle type	q	f ($\times 10^{49}$ ergs)
Proton	2.24	6.95
Helium	2.21	0.79
Carbon	2.21	2.42×10^{-2}
Oxygen	2.25	2.52×10^{-2}
Neon	2.25	3.78×10^{-3}
Magnesium	2.29	5.17×10^{-3}
Silicon	2.25	5.01×10^{-3}
Iron	2.25	4.95×10^{-3}

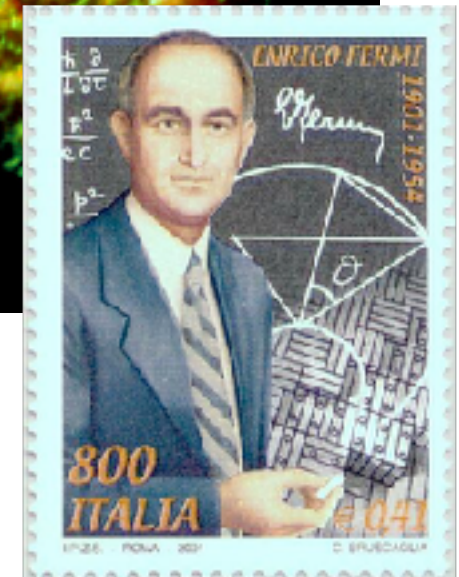
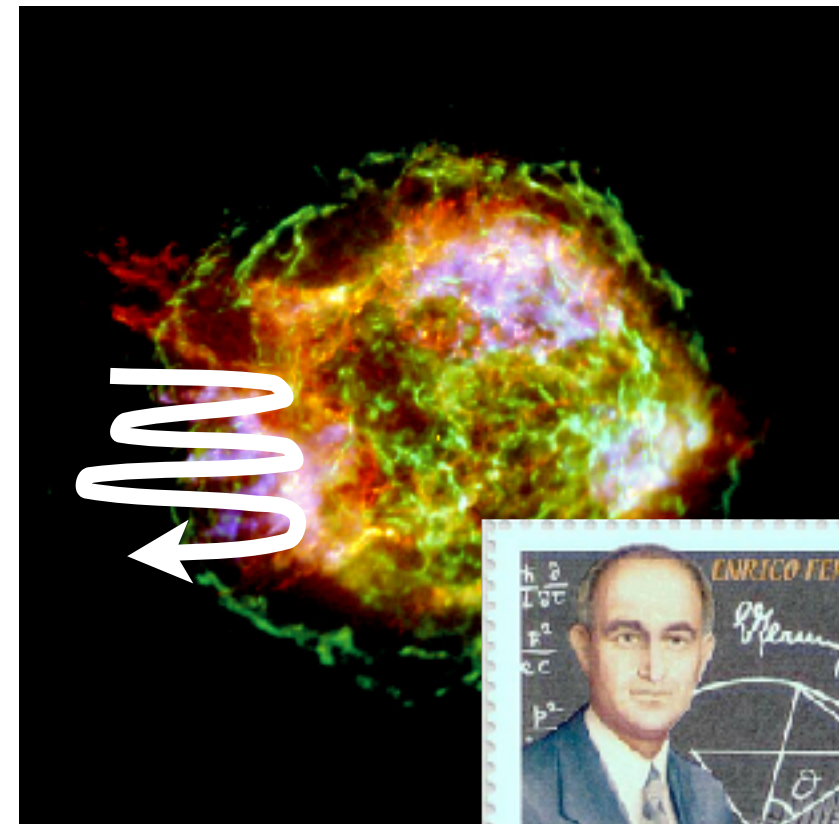




maximum energy

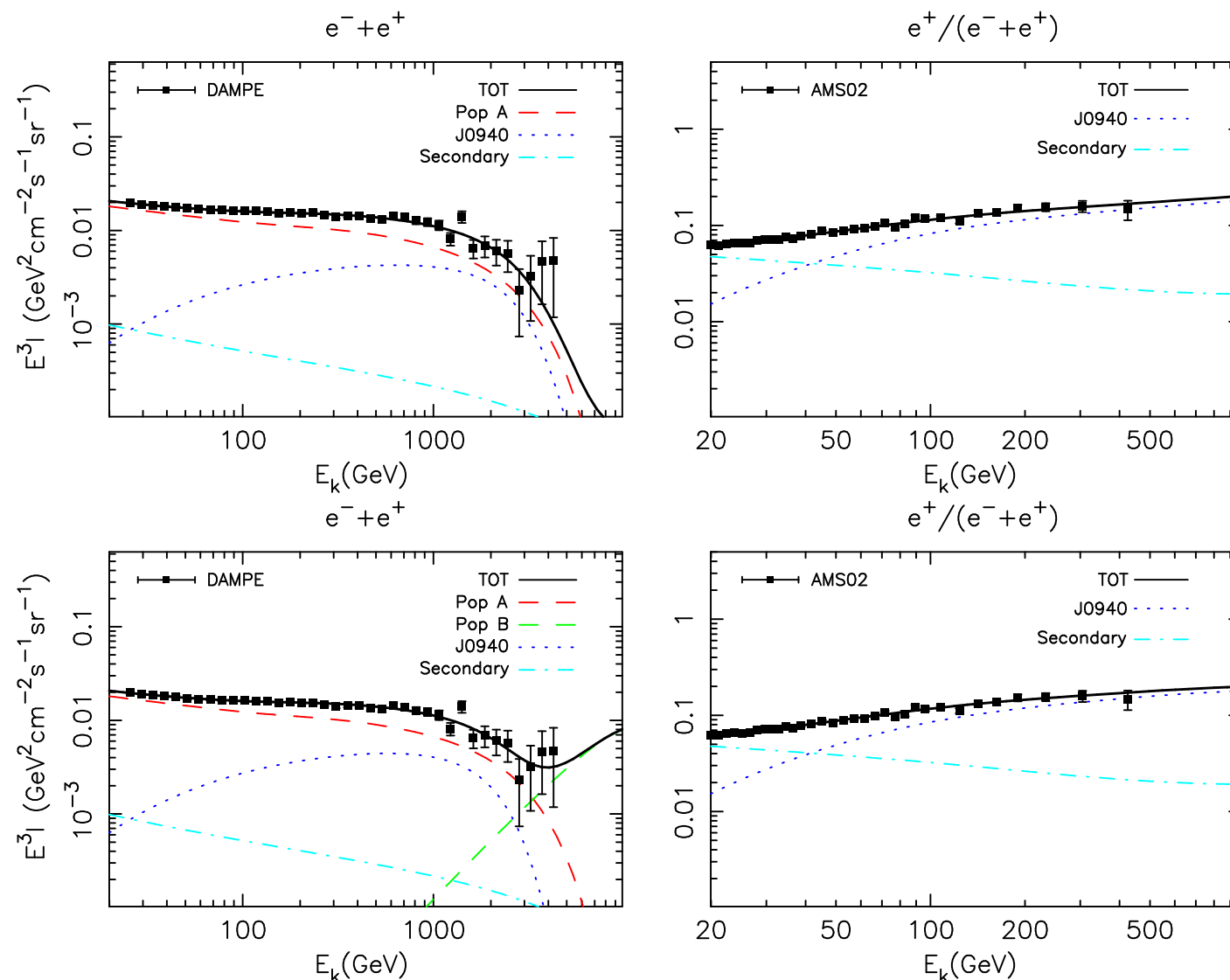
$$E_{max} \propto B \cdot Z$$

$$E_{max} \approx Z \cdot 100 \text{ TeV} \dots Z \cdot 5 \text{ PeV}$$



- Berezkhko
- . - . Kobayakawa
- ... Stanev
- Sveshnikova
- Poly Gonato

Explanation of the knee-like feature in the DAMPE cosmic $e^- + e^+$ energy spectrum



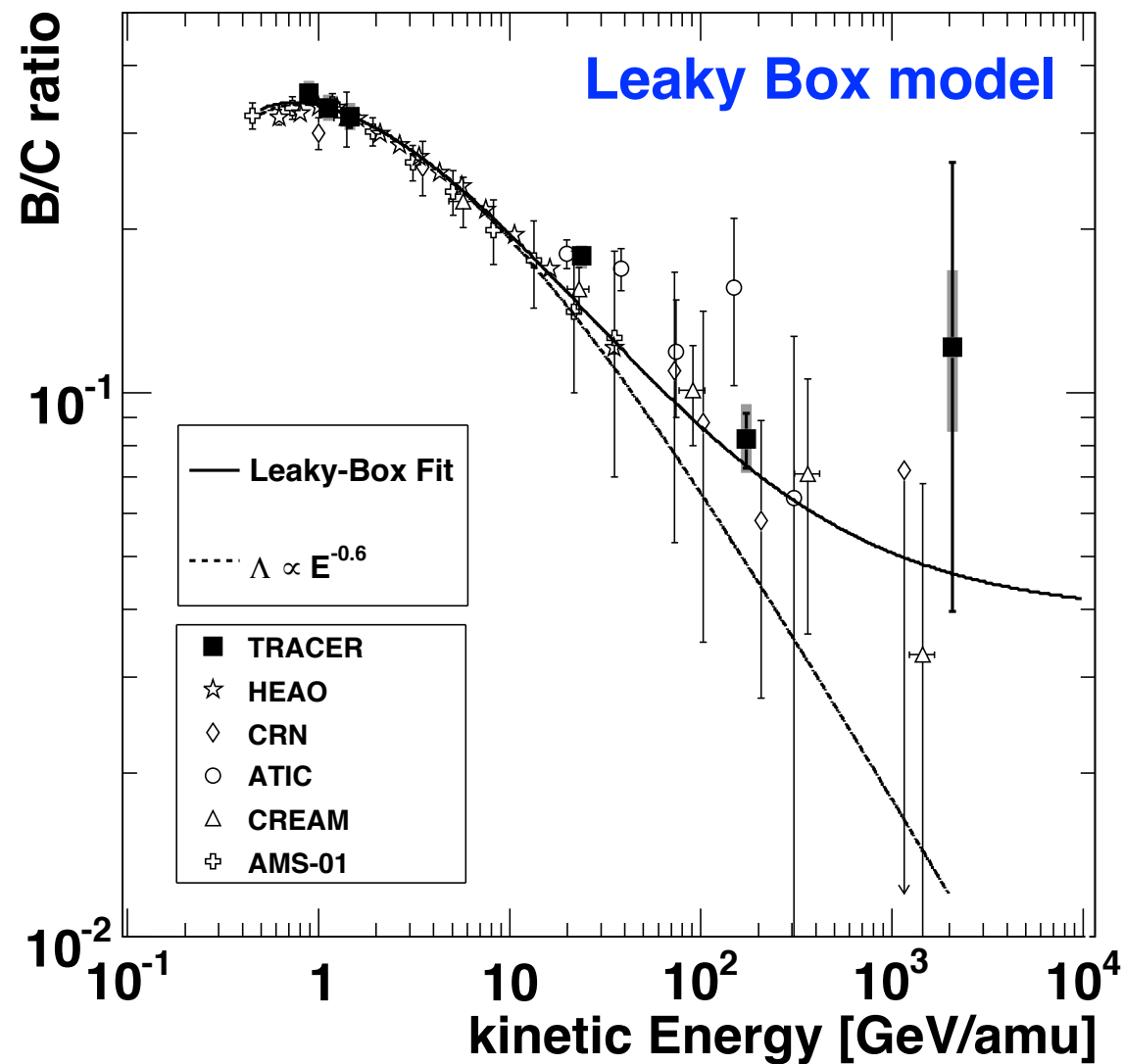
**acceleration of electrons in SNR
+ radiative cooling**

**(+maybe contribution from single
SNR)**

FIG. 1. Results of the fitting to the DAMPE $e^- + e^+$ and AMS-02 $e^+/(e^- + e^+)$ data, with PSR J0940-5428 as the single positron source in the high energy region. Left panels: the electron plus positron spectrum. Right panels: the positron fraction. The results in the bottom panels include the population B of SNRs, while the results in the top panels do not. In the legends, 'TOT' stands for the total $e^- + e^+$ flux (or $e^+/(e^- + e^+)$) of all the sources, the population A of SNRs are abbreviated to 'Pop A', the population B are abbreviated to 'Pop B', while 'J0940' stands for PSR J0940-5428.

Pathlength of cosmic rays in Galaxy

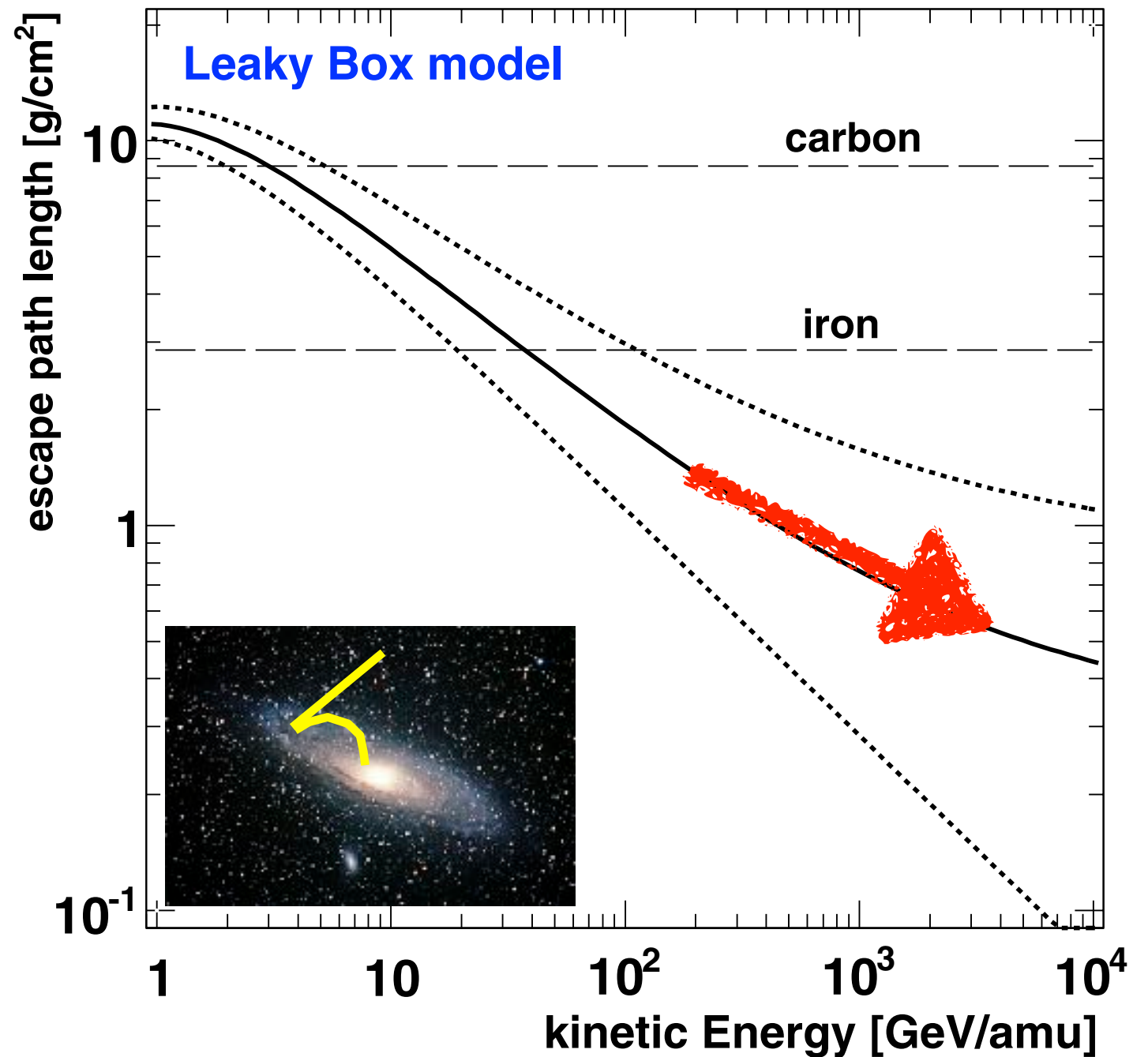
TRACER balloon experiment



Escape Path Length:

$$\Lambda_{esc}(E) = CE^{-\delta} + \Lambda_0$$

- Propagation index:
 $\delta = 0.64 \pm 0.02$.
- Residual path length:
 $\Lambda_0 = 0.7 \pm 0.2 \text{ g/cm}^2$.



$$\Lambda(R) = \frac{26.7\beta}{(\beta R)^\delta + (0.714 \cdot \beta R)^{-1.4}} + \Lambda_0 \text{ g/cm}^2,$$

Propagation of super-high-energy cosmic rays in the Galaxy

Jörg R. Hörandel ^{a,*}, Nikolai N. Kalmykov ^b, Aleksei V. Timokhin ^c

The steady-state diffusion equation for the cosmic-ray density $N(r)$ is (neglecting nuclear interactions and energy losses)

$$-\nabla_i D_{ij}(r) \nabla_j N(r) = Q(r). \quad (1)$$

$Q(r)$ is the cosmic-ray source term and $D_{ij}(r)$ the diffusion tensor.

Under the assumption of azimuthal symmetry and taking into account the predominance of the toroidal component of the magnetic field, Eq. (1) is presented in cylindrical coordinates as

$$\left[-\frac{1}{r} \frac{\partial}{\partial r} r D_{\perp} \frac{\partial}{\partial r} - \frac{\partial}{\partial z} D_{\perp} \frac{\partial}{\partial z} - \frac{\partial}{\partial z} D_A \frac{\partial}{\partial r} + \frac{1}{r} \frac{\partial}{\partial r} r D_A \frac{\partial}{\partial z} \right] N(r, z) = Q(r, z), \quad (2)$$

where $N(r, z)$ is the cosmic-ray density averaged over the large-scale fluctuations with a characteristic scale $L \sim 100$ pc [3]. $D_{\perp} \propto E^m$ is the diffusion coefficient, where m is much less than one ($m \approx 0.2$), and $D_A \propto E$ the Hall diffusion coefficient. The influence of Hall diffusion becomes predominant at high energies ($>10^{15}$ eV). The sharp

The magnetic field of the Galaxy consists of a large-scale regular and a chaotic, irregular component $\vec{B} = \vec{B}_{\text{reg}} + \vec{B}_{\text{irr}}$. A purely azimuthal magnetic field was assumed for the regular field

$$B_z = 0, \quad B_r = 0, \quad B_{\phi} = 1 \mu\text{G} \exp\left(-\frac{z^2}{z_0^2} - \frac{r^2}{r_0^2}\right),$$

where $z_0 = 5$ kpc and $r_0 = 10$ kpc are constants [3].

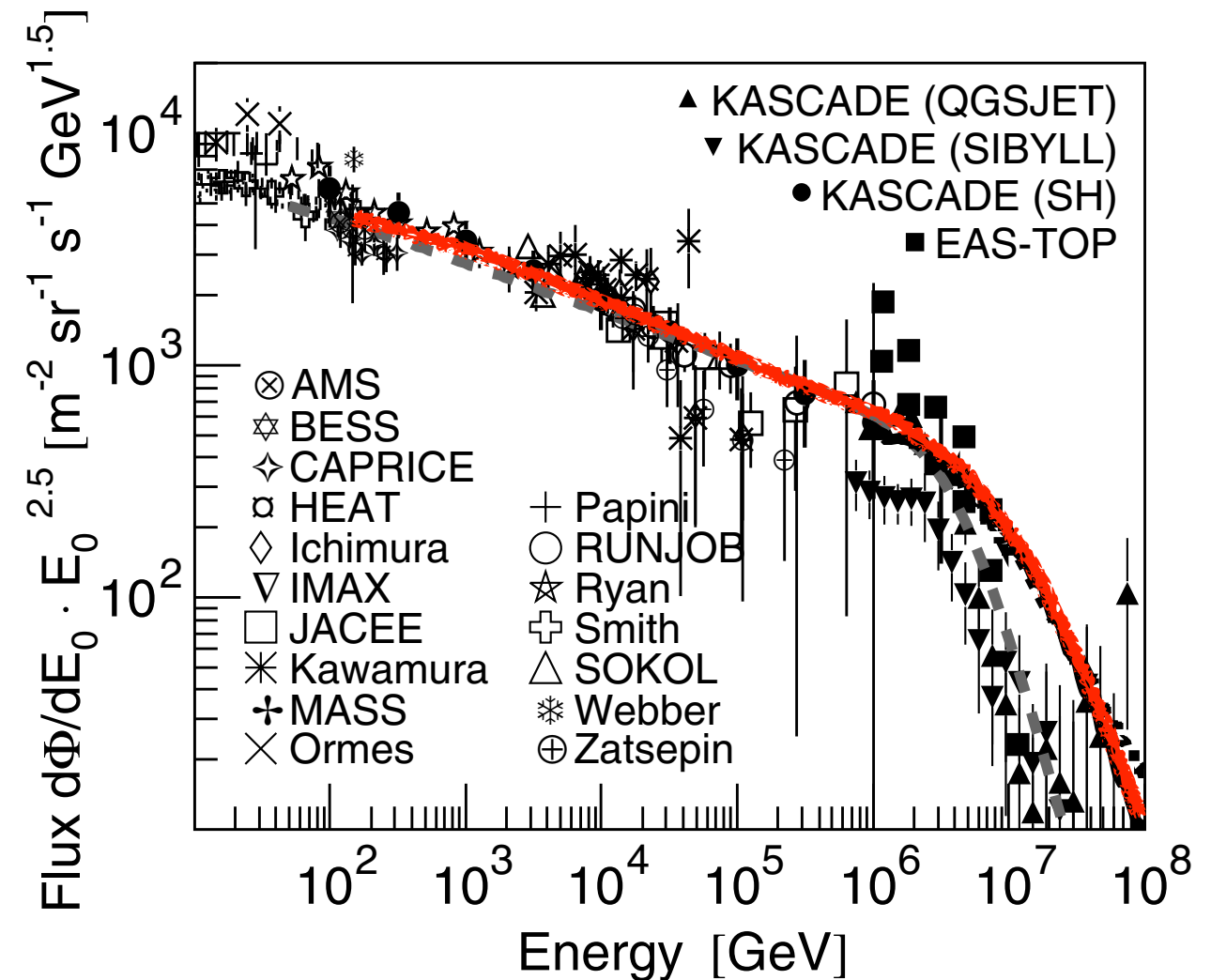


Fig. 7. Proton flux as obtained from various measurements, for references see [28], compared to the spectra shown in Fig. 6 (black lines) and the *polygonoato* model [26] (grey, dashed line).

Cosmic-Ray Transport between the Knee and the Ankle with CRPropa

Lukas Merten^{*a}, Julia Tjus^a, Chad Bustard^b, and Ellen G. Zweibel^{bc}

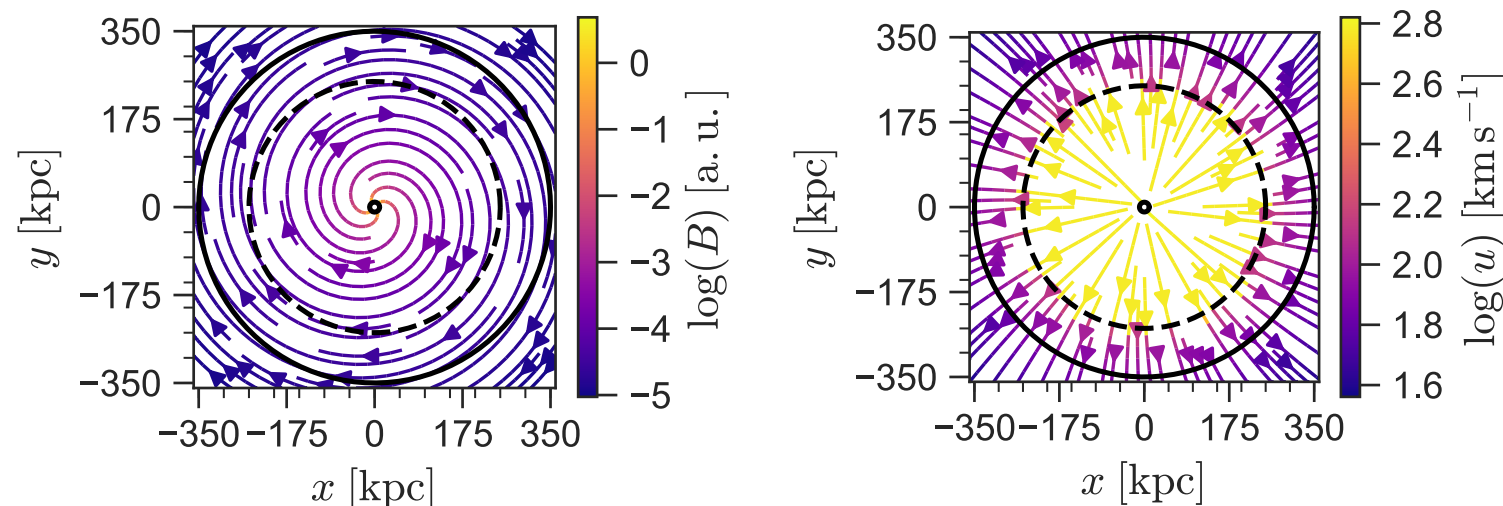


Figure 1: Face on view of the magnetic field and the Galactic wind in the Galactic plane. The inner solid circle is the observer sphere and the outer solid circle is the free escape boundary. The shock position is marked by the dashed circle.

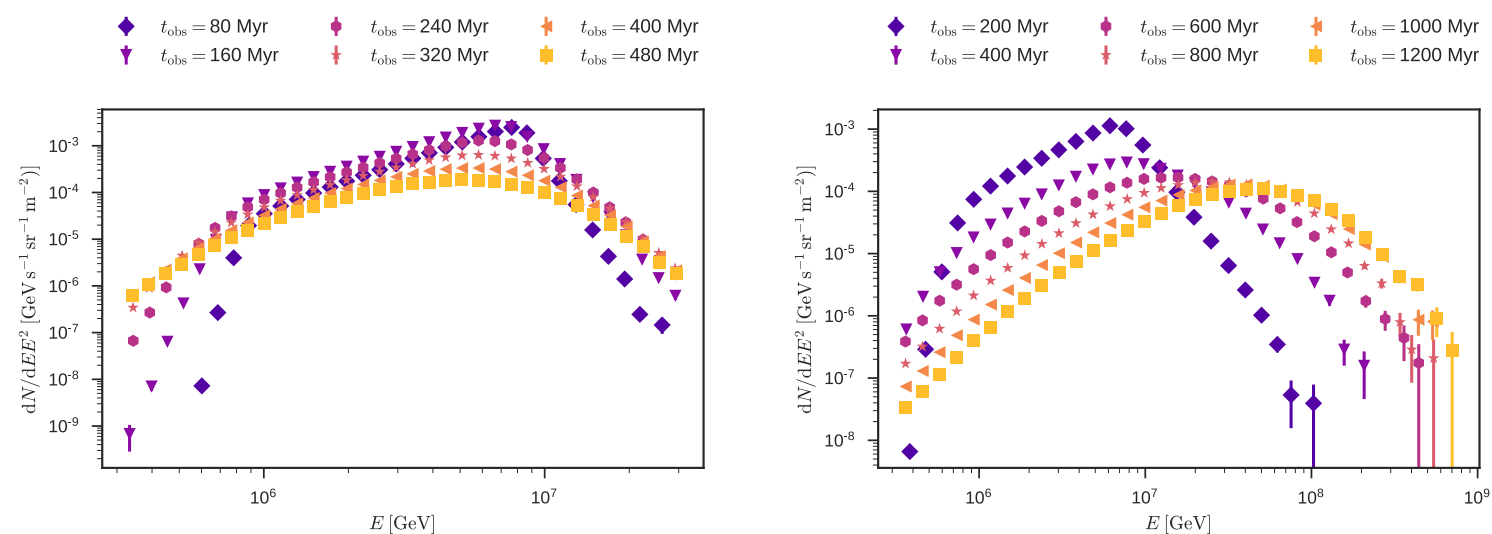


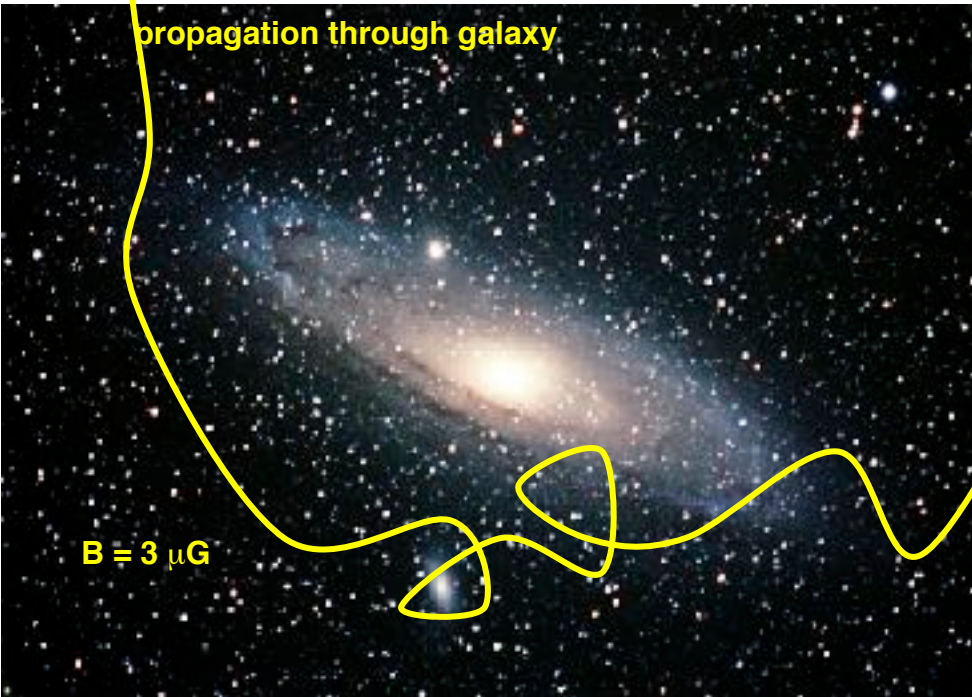
Figure 2: Energy spectrum at the spherical observer sphere $r_{\text{obs}} = 10$ kpc. Left including perpendicular diffusion $\epsilon = 0.1$ and right pure parallel diffusion.

In this work an innovative technique—based on stochastic differential equations—to solve the transport equation is explained.

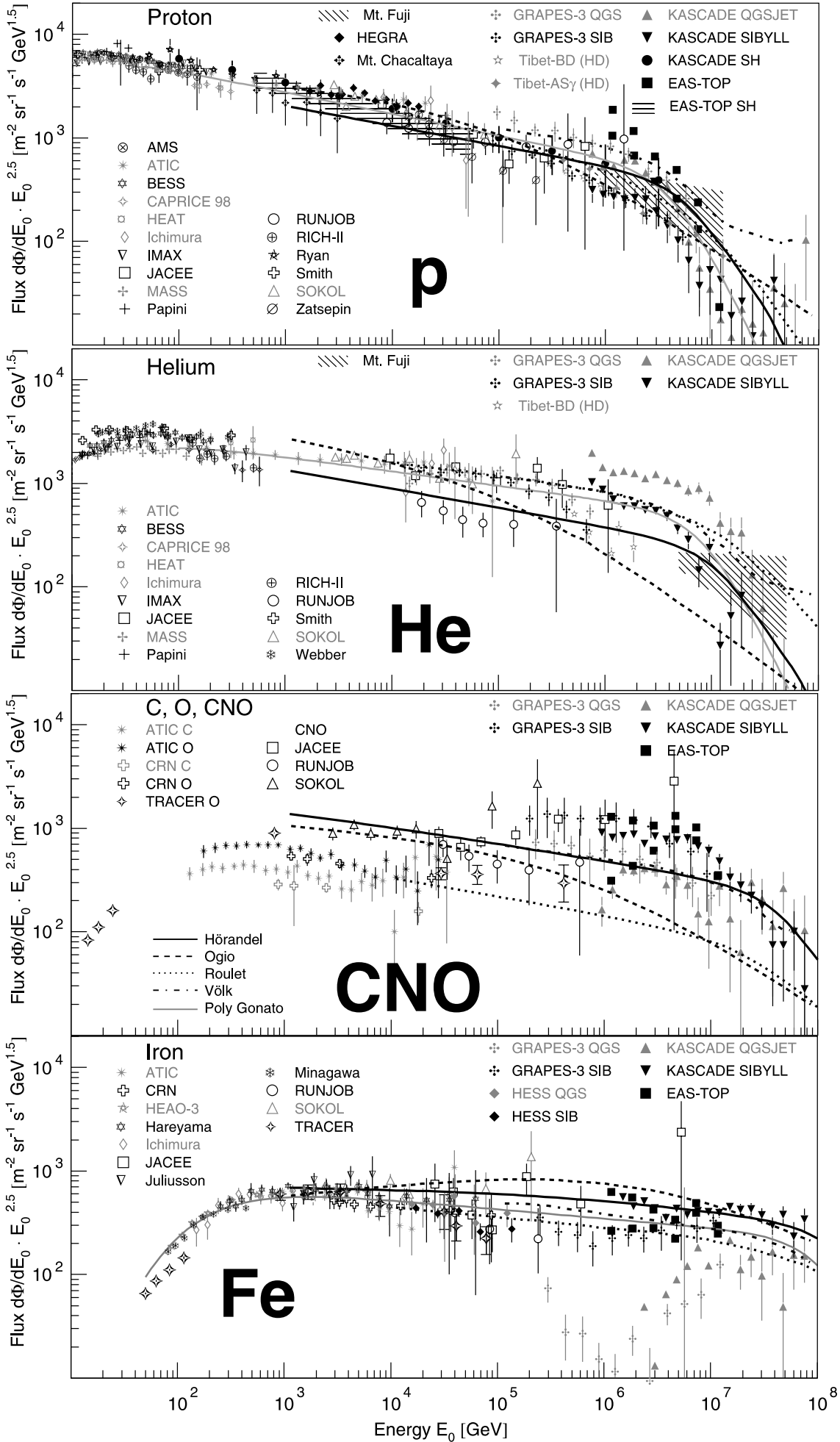
The ansatz of propagating independent phase-space elements (or pseudo-particles) allows for easy parallelization which makes it attractive for modern large-scale computing architectures. It combines the numerical framework of the single particle propagation with the advantage of ensemble averaged description of the transport equation. Making it an ideal tool to describe the transition between Galactic and extra-galactic cosmic-rays.

leakage from Galaxy

$$E_k \propto Z$$

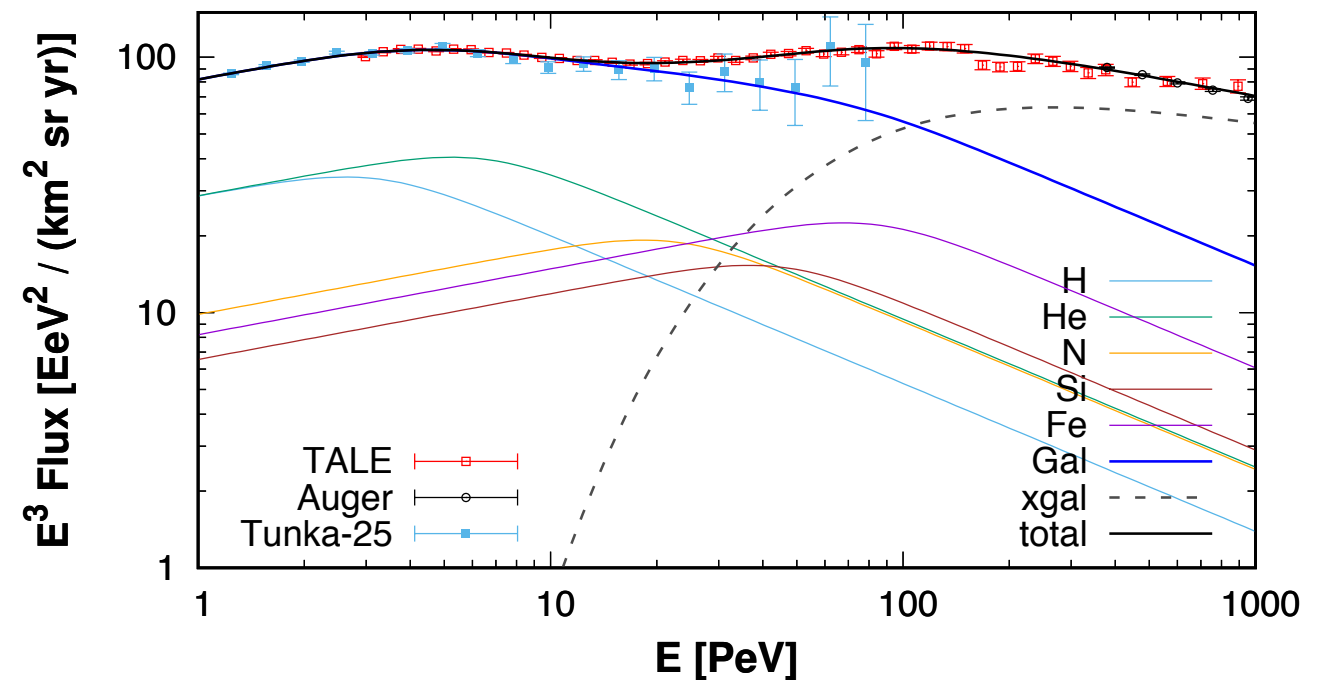
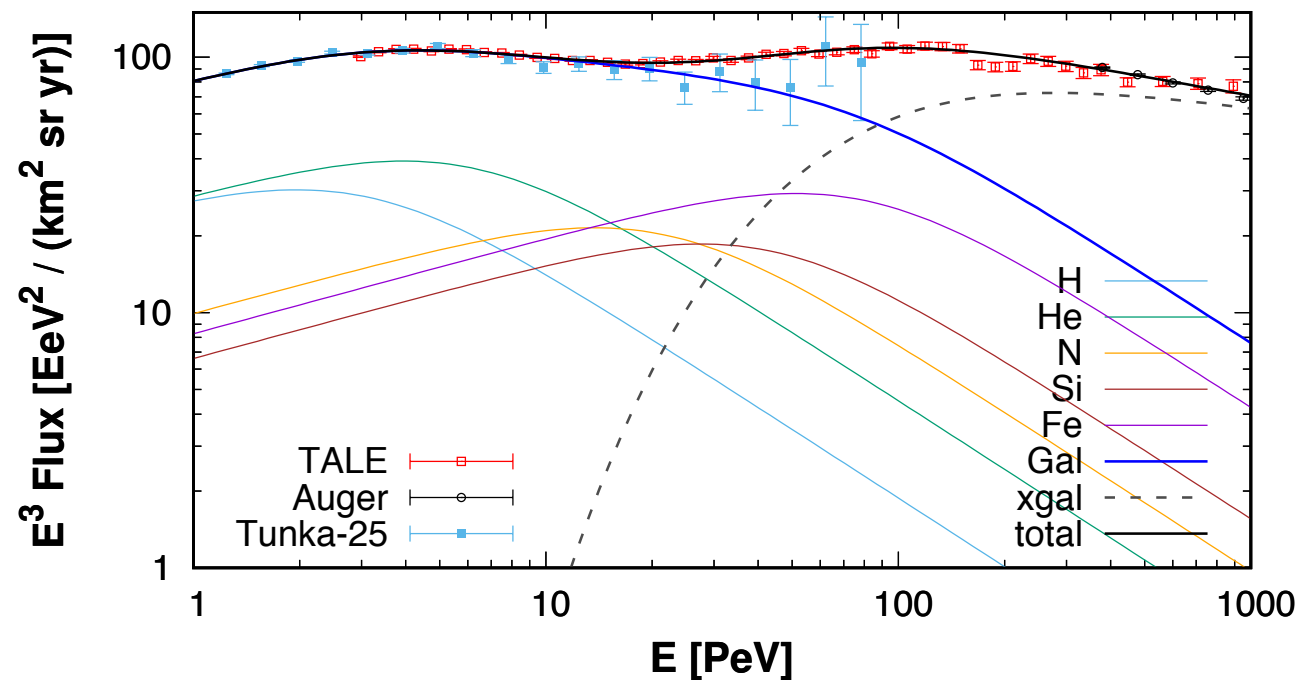
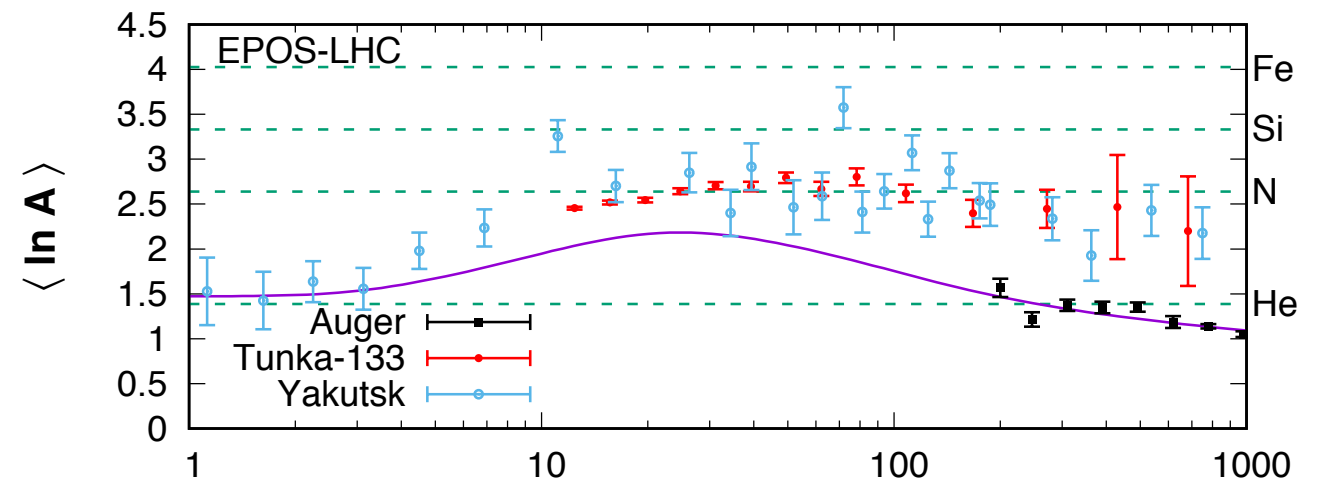
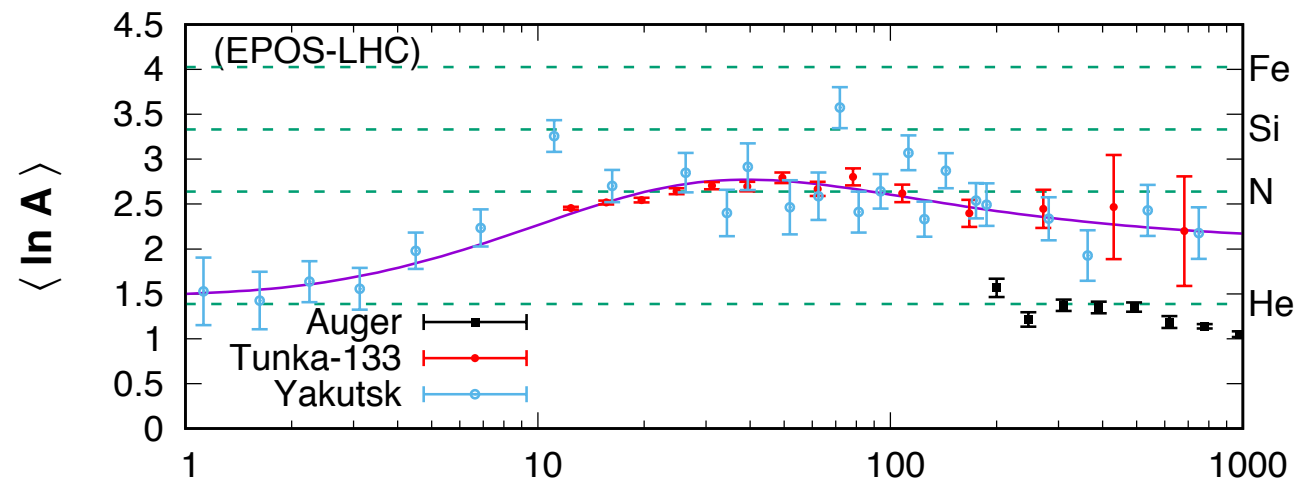


- Hörandel
- - - Ogio
- Roulet
- . - . Völk
- Poly Gonato



A scenario for the Galactic cosmic rays between the knee and the second-knee

fit using X_{\max} data from TALE, Tunka, Yakutsk, Auger

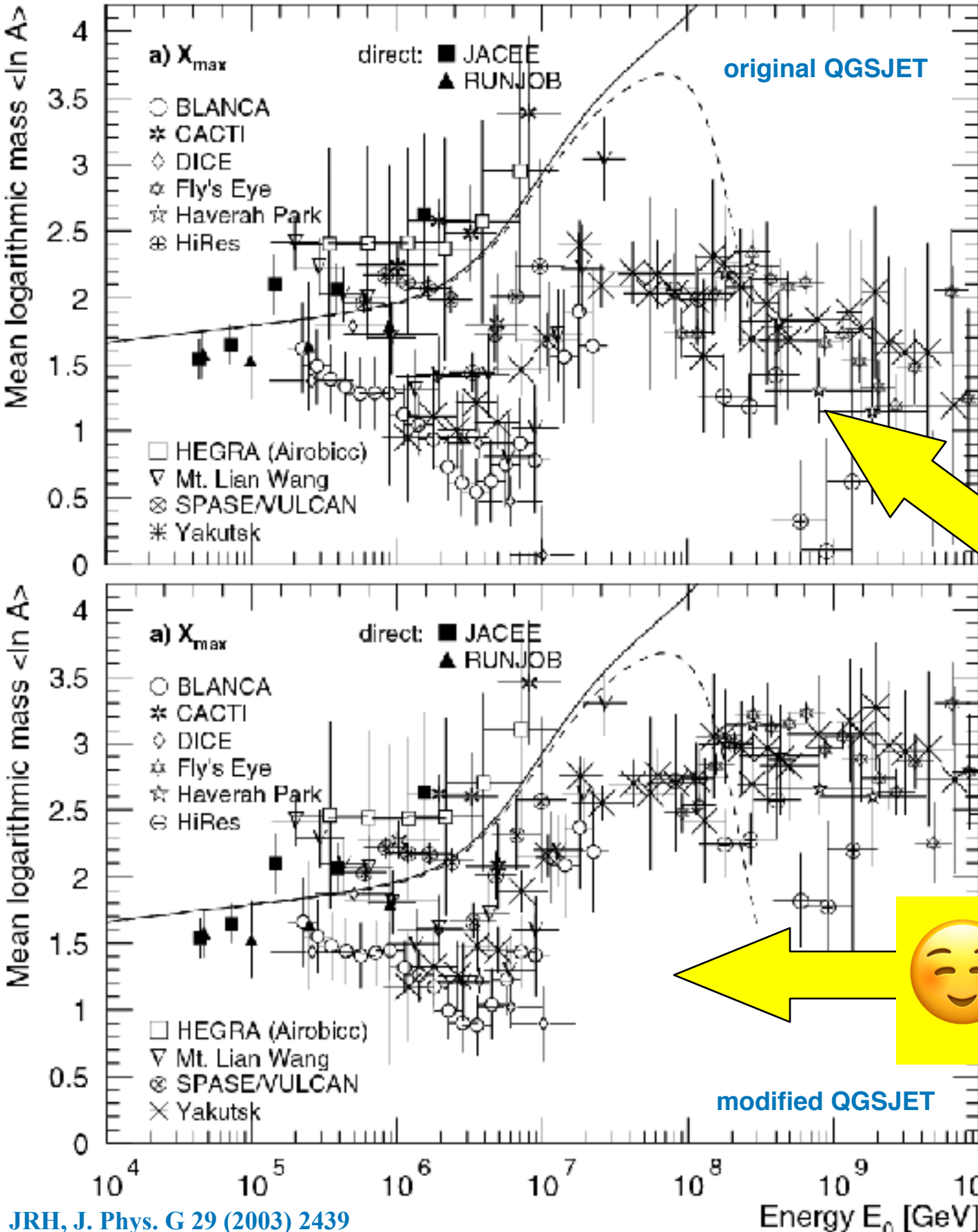


knee at $E_k \sim 3 \text{ PeV} * Z$
 \rightarrow Fe knee at 80 PeV

extragalactic component dominant $>100 \text{ PeV}$

Mean logarithmic mass

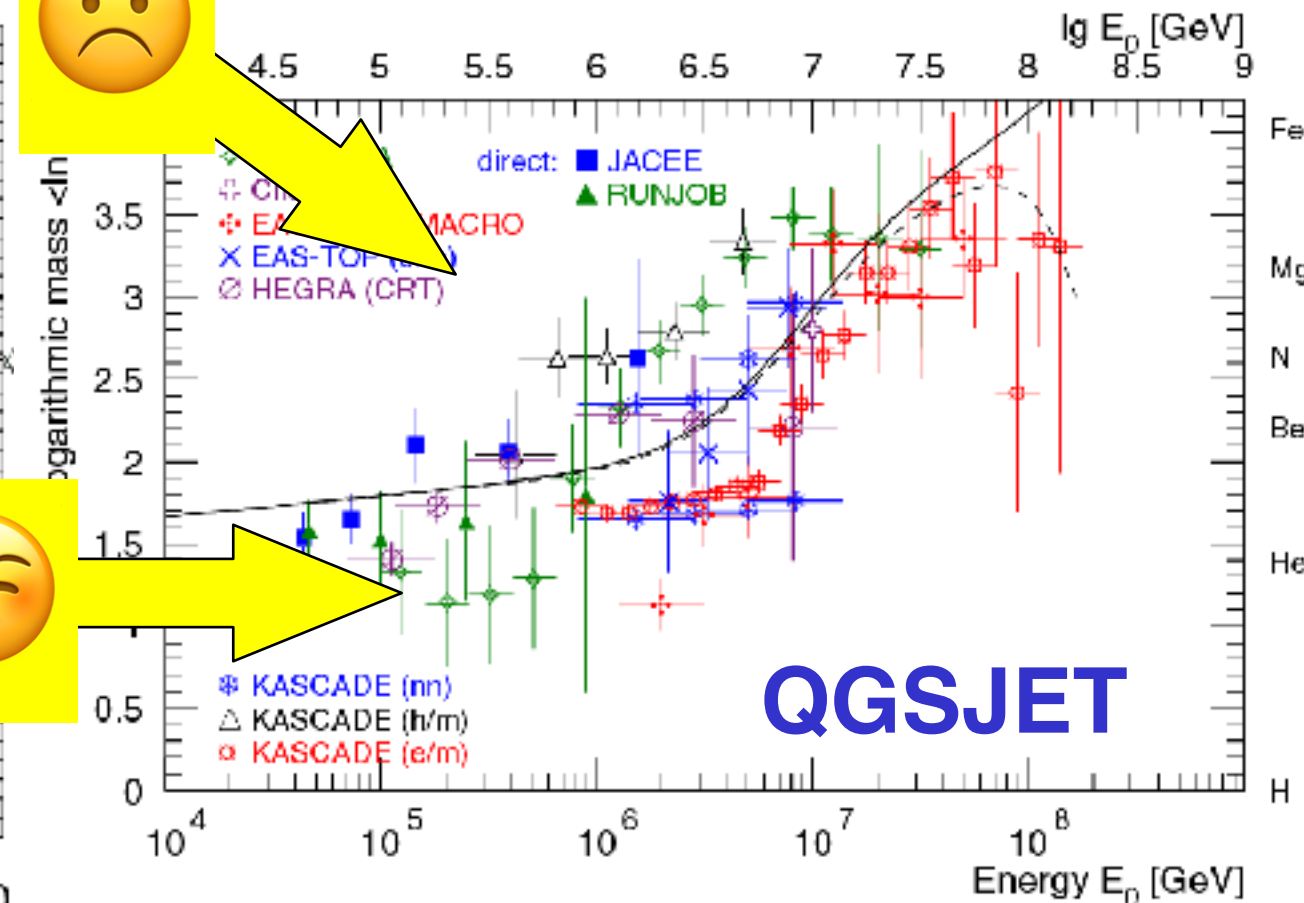
X_{\max}



discrepancy between X_{\max} measurements and particles at ground (e, μ , h)
Inconsistencies in EAS simulations - longitudinal vs. lateral development

→ *hadr. cross section, inelasticity*

electrons, muons, hadrons



Contribution of (regular) SNR-CR to all-particle spectrum

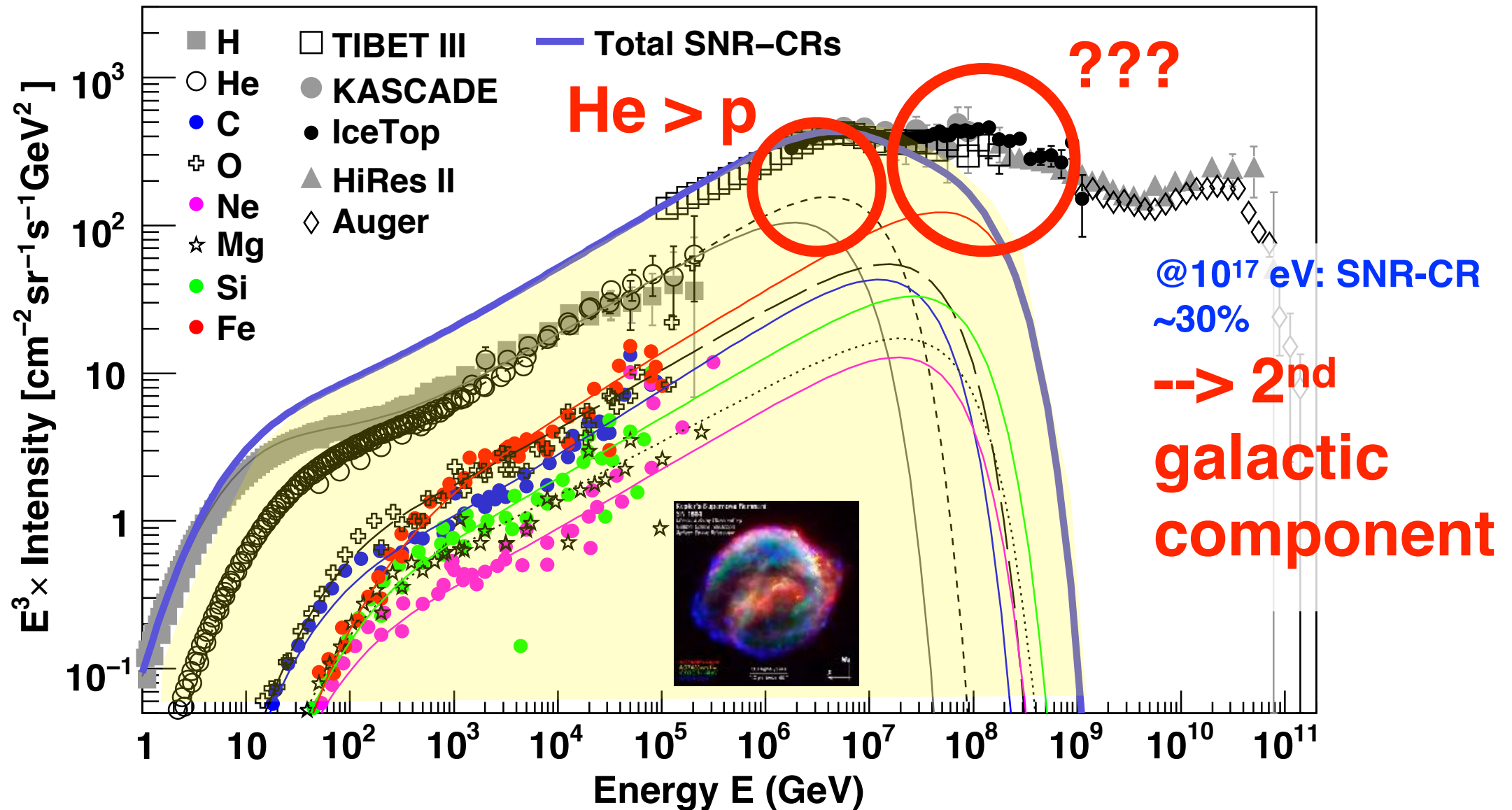
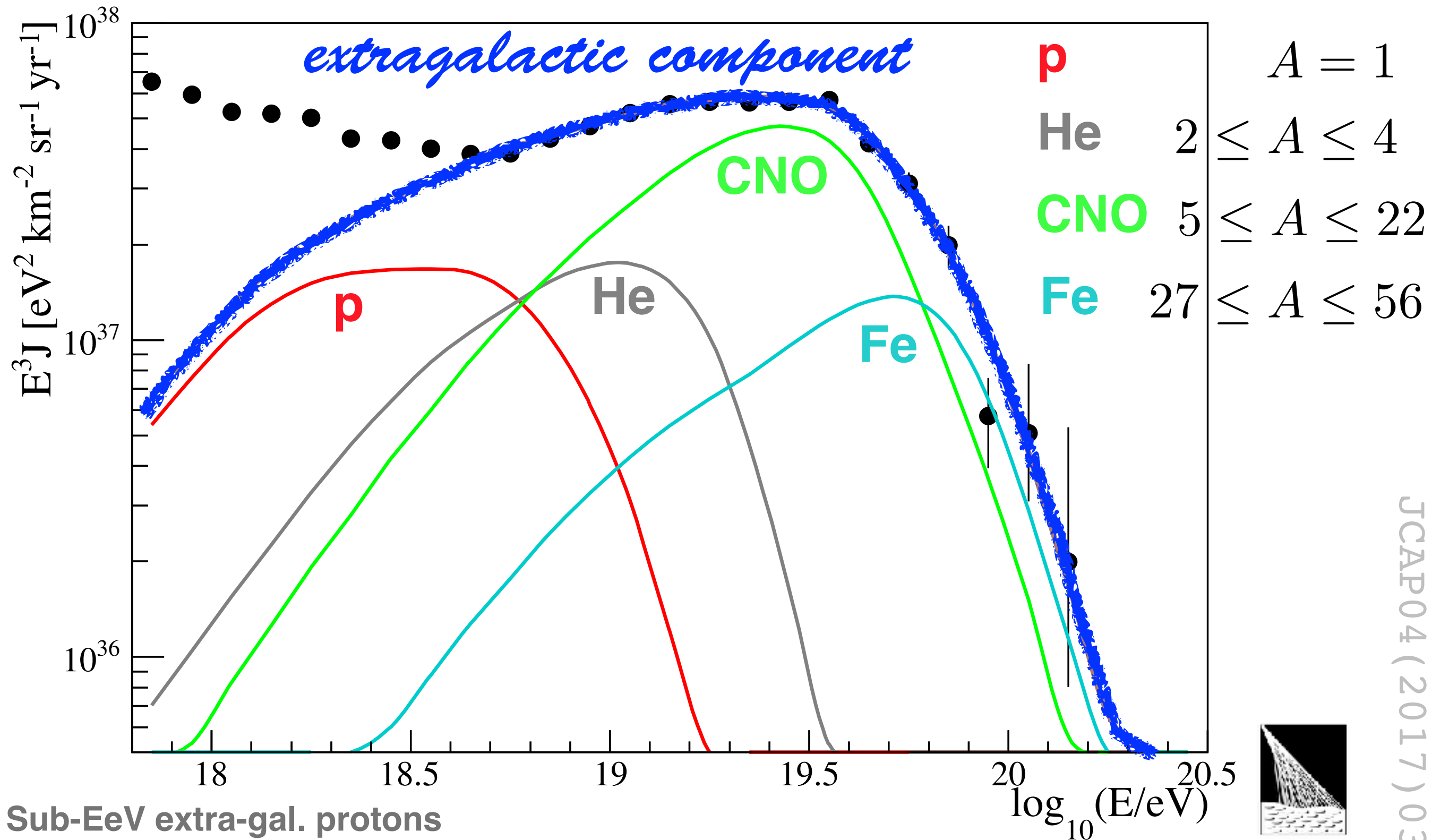


Fig. 2. Contribution of SNR-CRs to the all-particle cosmic-ray spectrum. The thin lines represent spectra for the individual elements, and the thick-solid line represents the total contribution. The calculation assumes an exponential cut-off energy for protons at $E_c = 4.5 \times 10^6$ GeV. Other model parameters, and the low-energy data are the same as in Figure 1. Error bars are shown only for the proton and helium data. High-energy data: KASCADE (Antoni et al. 2005), IceTop (Aartsen et al. 2013), Tibet III (Amenomori et al. 2008), the Pierre Auger Observatory (Schulz et al. 2013), and HiRes II (Abbasi et al. 2009).

~8% of mechanical power of SN --> CRs

Combined fit of spectrum and
composition data as measured by the
Pierre Auger Observatory



Sub-EeV extra-gal. protons
from interactions of heavier
nuclei



all-particle spectra including 2nd galactic component

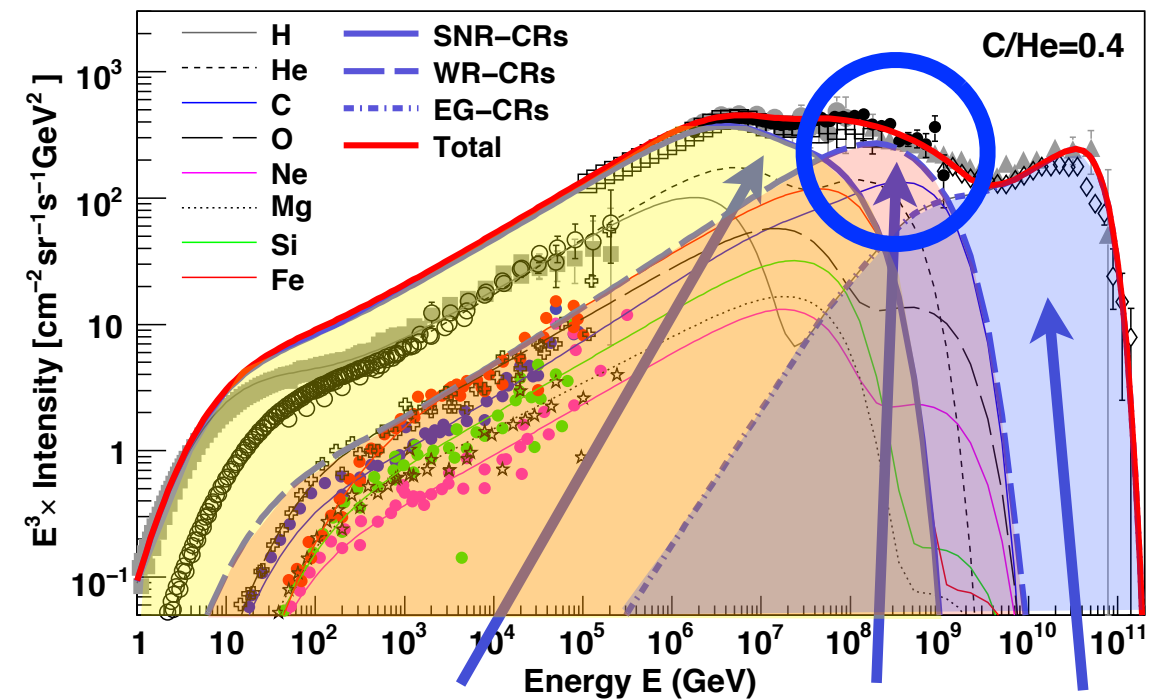
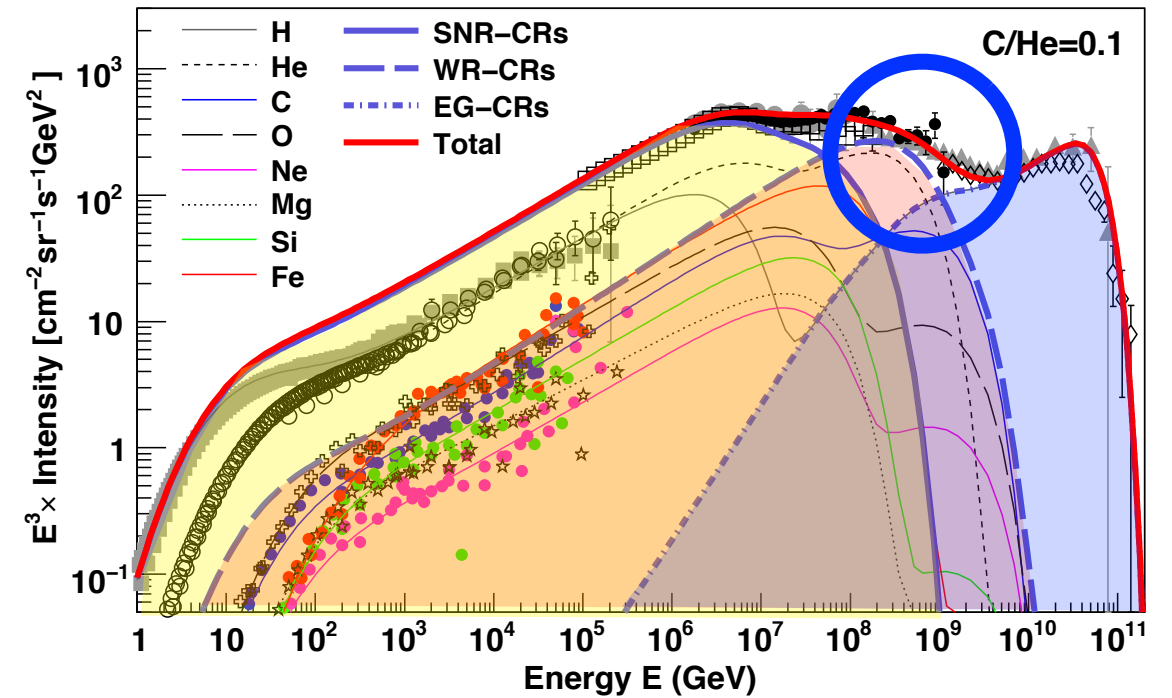
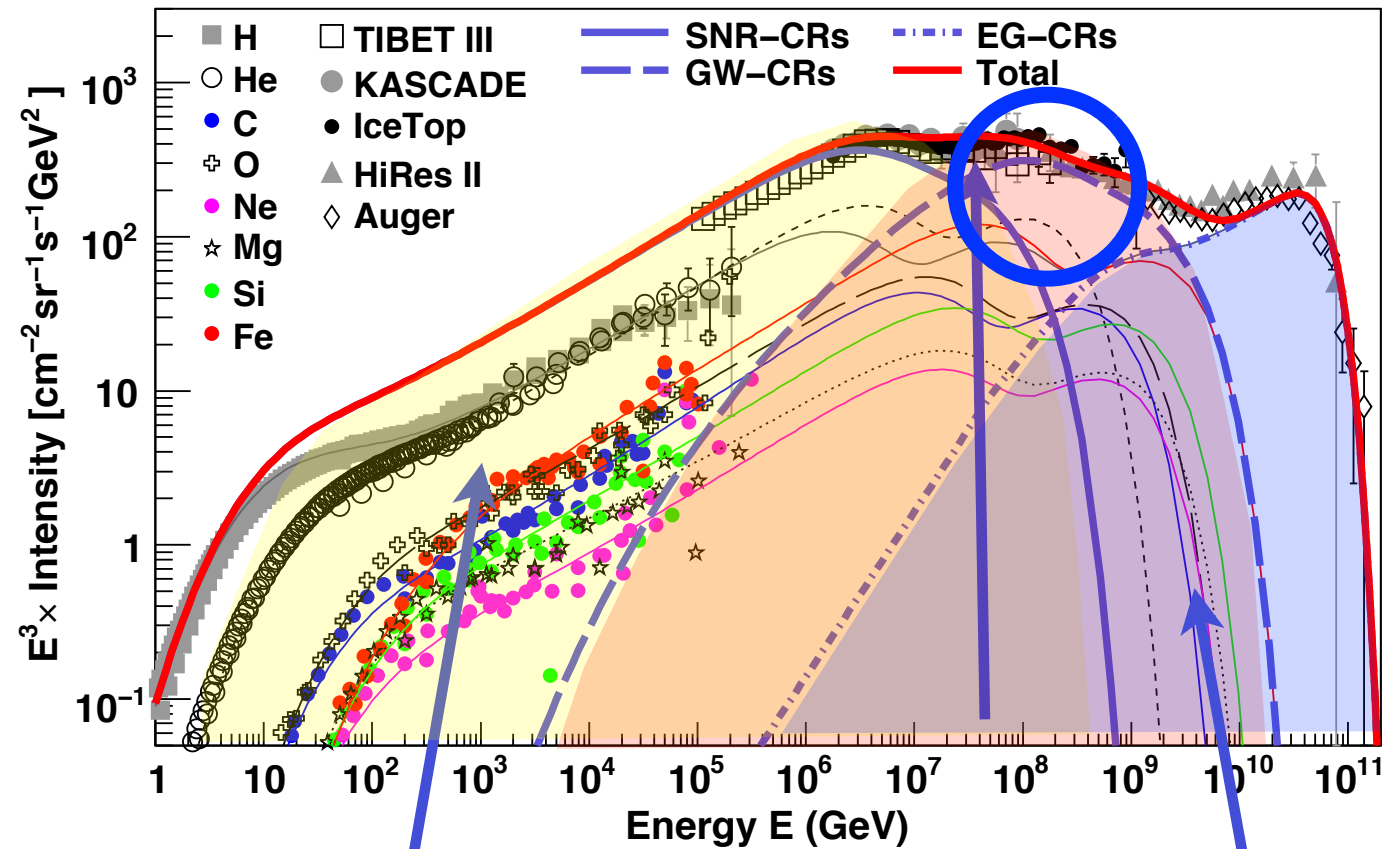
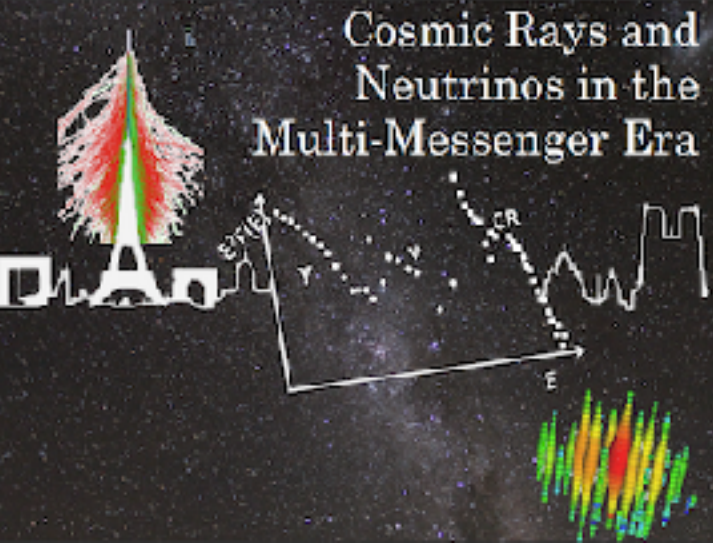


Table 3. Injection energy of SNR-CRs used in the calculation of all-particle spectrum in the WR-CR model (Figure 6).

Particle type	C/He = 0.1 $f(\times 10^{49} \text{ ergs})$	C/He = 0.4 $f(\times 10^{49} \text{ ergs})$
Proton	8.11	8.11
Helium	0.67	0.78
Carbon	2.11×10^{-2}	0.73×10^{-2}
Oxygen	2.94×10^{-2}	2.94×10^{-2}
Neon	4.41×10^{-3}	4.41×10^{-3}
Magnesium	6.03×10^{-3}	6.03×10^{-3}
Silicon	5.84×10^{-3}	5.84×10^{-3}
Iron	5.77×10^{-3}	5.77×10^{-3}



Paris
7-11 December 2020



Nikhef



Models for the knee in the energy spectrum of cosmic rays

- knee in all-particle spectrum at ~ 4.5 PeV caused by fall-off of light elements (p, He)
- experimental (world) data indicate rigidity-dependent fall-off of individual elements
(in particular unfolding by KASCADE[-Grande] and IceCube/Top)
- spectrum above knee is superposition of individual spectra (elemental knees)
 - > fine structure in all-particle spectrum
 - > end of galactic CR component
- astrophysical origin of knee:
combination of maximum energy attained in sources (Supernovae) (Hillas criterion)
and leakage from Galaxy
- 2nd galactic component at $\sim 10^{17}$ eV?
- extra-galactic origin $> 10^{18}$ eV